INSTITUTO SUPERIOR DE ENGENHARIA DO PORTO
MESTRADO EM ENGENHARIA BIOMÉDICA

Bioprinting strategies to engineer biomimetic 3D models of skin burn wounds

LUÍS MIGUEL BRUNHOSO BEBIANO
Outubro de 2022

P.PORTO

Bioprinting strategies to engineer biomimetic 3D models of skin burn wounds

Luís Miguel Brunhoso Bebiano

Bachelor's Degree in Biomedical Engineering at Instituto Superior de Engenharia do Porto

"Dissertation presented at Instituto Superior de Engenharia do Porto to obtain the Master Degree in Biomedical Engineering"

Advsiors at i3S: Prof. Dr. Rúben Pereira, ICBAS/i3S & Dr. Bruno Pereira, i3S/IPATIMUP

Advsior at ISEP: Dra. Cristina Ribeiro

October 2022

Acknowledgements

At the end of this thesis, there are a lot of people that I would like to thank. One way or another, they all contributed to the development of this work.

I would like to express my deepest gratitude to my supervisors Dr. Rúben Pereira, Dr. Bruno Pereira and Dra. Cristina Ribeiro for the opportunity, unconditional support and competence guidance provided during the realization of this thesis.

Thanks to all my friends and my partner for their support and motivation. I also want to thank all my colleagues from the Biofabrication group for their knowledge sharing, support and help.

Lastly, and most importantly, I would like to express my sincere thanks to my entire family. My parents for all the education and being present when I needed the most. My brother João for all the patience and memories. My cousin Pedro for all the support and advices. A special mention also goes for my uncles for always supporting me. This dissertation is dedicated to all of them, including my deceased grandparents, who are extremely happy for the conclusion of this journey.

Resumo

As queimaduras da pele são consideradas um grave problema de saúde pública em todo o mundo, sendo uma das principais causas de morbidade, dor e, em alguns casos, desfiguração do paciente. Apesar de existirem terapias comercialmente disponíveis, como os curativos modernos e os substitutos da pele, ainda existem limitações críticas no que respeita ao desenvolvimento de terapias mais eficazes que possam diminuir a ocorrência de fibrose e melhorar os resultados estéticos e funcionais. Para tal, torna-se crucial melhorar a nossa compreensão sobre as respostas e mecanismos a nível celular e da matriz extracelular (MEC) que ocorrem após a lesão.

Com o objetivo de endereçar as limitações mencionadas, uma nova *bioink* constituída por um único polímero foi desenvolvida para criar modelos 3D *in vitro* relevantes a nível patofisiológico de queimaduras da pele. Inicialmente, uma *bioink* derivada de pectina e funcionalizada com grupos funcionais maleimida foi desenvolvida usando uma estratégia de reticulação dupla através de gelificação iónica e da reação de adição de Michael. Esta estratégia permitiu não só modular as propriedades mecânicas (2593.00 ± 261.50 até 5860.00 ± 386.10 Pa) dos hidrogéis na gama de valores da pela nativa, mas também recriar importantes propriedades da MEC da pele a nível bioquímico e biofísico. Um estudo sistemático foi realizado para avaliar a influência de agentes reticulantes degradáveis ou não degradáveis através das metaloproteinases da matriz nas propriedades do hidrogel e na resposta celular. Curiosamente, todas as formulações permitiram a formação de hidrogéis com uma distribuição uniforme de fibroblastos da derme em 3D, embora os resultados sugiram que os hidrogéis degradáveis permitem uma maior formação de redes celulares interconectadas. Além disso, os hidrogéis degradáveis também aumentaram a deposição de componentes da MEC em comparação com os hidrogéis não degradáveis.

Para criar um modelo *in vitro* 3D de pele em bicamada, os queratinócitos foram cultivados na parte superior de hidrogéis contendo fibroblastos (derme), e mantidos em cultura por 28 dias. Após este período de tempo, um modelo de pele *in vitro* estruturalmente semelhante à pele nativa foi obtido e usado para criar de forma eficiente um modelo 3D de queimadura de pele usando uma vara de aço inoxidável a 65 °C durante 120s. Especificamente, a abordagem experimental desenvolvida permitiu induzir uma queimadura caracterizada por morte celular localizada, ou seja, dentro da

região da queimadura, sem afetar a viabilidade celular na região saudável circundante. De facto, o ensaio de *Live/Dead* sugere que a resposta celular na região da queimadura é dependente do tempo uma vez que células mortas foram detetadas apenas num período tardio após a lesão (7 dias), mas não ao dia 1 pós-lesão.

Por último, uma estratégia de bioimpressão 3D foi implementada para criar um hidrogel que permita a perfusão diretamente num chip personalizado gerado por impressão 3D. Esta estratégia permitiu demonstrar a integração das abordagens experimentais desenvolvidas na dissertação com a finalidade de gerar modelos 3D vascularizados de queimaduras de pele. No geral, neste trabalho é reportado pela primeira vez o desenvolvimento de um modelo biomimético de pele *in vitro* recapitulando as principais características de queimaduras de pele com resultados promissores para aplicações de engenharia de tecidos, incluindo a reprodução de patologias de pele, o teste de fármacos e a cicatrização de feridas.

Palavras-chave: Bioimpressão 3D; *Click Chemistry*; Hidrogel; Modelo de pele 3D; Pele; Queimadura de pele

Abstract

Skin burns are considered a major public health problem worldwide, being a leading cause of patient morbidity, pain, and, in some cases, disfigurement. Despite several therapies being commercially available, such as modern dressings and skin substitutes, there are still critical limitations regarding the development of more effective therapies that can diminish the occurrence of fibrosis and improve both aesthetic and functional outcomes. To do that, it is crucial to improve our understanding regarding the responses and mechanisms at cellular and extracellular matrix (ECM) level occurring upon injury.

To address the mentioned limitations, herein a novel single-polymer bioink was developed to engineer pathophysiological relevant *in vitro* 3D models of skin burn wounds. First, a maleimide-functionalized pectin derivative (PectX-MAL) bioink was developed by using a dual-crosslinked strategy comprising ionic gelation and thiol-Michael addition click chemistry. This strategy allowed not only to modulate the mechanical properties (2593.00 ± 261.50 to 5860.00 ± 386.10 Pa) of dual-crosslinked hydrogels in the range of native skin, but also to resemble other key biophysical and biochemical cues of skin ECM. A systematic study was carried out to evaluate the influence of degradable and non-degradable biscysteine crosslinkers on hydrogel properties and cellular response. Interestingly, all formulations allowed the spreading of dermal fibroblasts, though results suggest that degradable hydrogels further stimulate cell spreading. Furthermore, degradable hydrogels also increased the deposition of ECM components in comparison to the non-degradable hydrogels.

In order to create an *in vitro* bilayer skin model, keratinocytes were seeded on top of a fibroblast-laden hydrogel and cultured for 28 days. After this time period, an *in vitro* skin model structurally similar to the native skin was obtained and used to efficiently create a 3D skin burn wound model by using a stainless-steel rod at 65 °C for 120s. Specifically, the developed experimental setup allowed to induce a burn wound characterized by site-specific cellular dead, i.e., within the burn area, while not affecting cellular viability in the surrounding unwounded region. Notably, Live/Dead assay suggests that cell response within the burn region is time-dependent as dead cells were only detected at a late time period after injury (7 days), but not at day 1 post-injury.

Finally, a bioprinting strategy was implemented to engineer a perfusable hydrogel in a customized 3D printed chip as a proof-of concept demonstration towards the generation of vascularized 3D models of skin burns. Overall, in this work the development of an *in vitro* skin biomimetic model recapitulating key hallmarks of skin burn wounds is reported for the first time with promising outcomes for tissue engineering applications, including disease modelling, drug screening and wound healing.

Keywords: 3D Bioprinting; 3D skin model; Burn wound; Click chemistry; Hydrogels; Skin

Funding

This work was carried out in the Biofabrication group at the Institute for Research and Innovation in Health Sciences (i3S) and was financed by European funds through European Regional Development Fund (ERDF), through COMPETE 2020 - Operational Programme for Competitiveness and Internationalisation (POCI), Portugal 2020, and by Portuguese funds through "Fundação para a Ciência e a Tecnologia" (FCT)/"Ministério da Ciência, Tecnologia e Inovação" in the framework of Project "Institute for Research and Innovation in Health Sciences" (Ref. POCI-01-0145-FEDER-007274), PTDC/MEC-GIN/29232/2017 and Portugal-UK Bilateral Research Fund (PARSUK/FCT).

List of Contents

List of Figures

List of Tables

List of Abbreviations

ABA	American Burn Association
AFS	Amniotic fluid-derived stem
ALI	Air-liquid interface
BSA	Bovine serum albumin
$CaCl_2$	Calcium chloride
CLSM	Confocal laser scanning microscope
D_2O	Deuterium oxide
dECM	Decellularized Extracellular matrix
DED	De-epidermized dermis
DMEM	Dulbecco's Modified Eagle Medium
DMTMM	4-(4,6-Dimethoxy-1,3,5-triazin-2-yl)-4-methylmorpholinium chloride
DTT	Dithiothreitol
ECM	Extracellular matrix
Ecs	Endothelial cells
EDTA	Ethylenediaminetetraacetic acid
EHS	Engelbreth-Holm-Swarm
FBS	Fetal bovine serum
FGF	Fibroblast growth factor
GAGs	Glycosaminoglycans
HA	Hyaluronic acid
HaCaT	Immortalized human keratinocytes
HBSS	Hank’s Balanced Salt Solution
H&E	Hematoxylin/Eosin
hNDFs	Dermal fibroblasts isolated from human neonatal foreskin
HSE	Human skin equivalent
MMP	Matrix metalloproteinases

MSCs	Mesenchymal stem cells
NaCl	Sodium chloride
NaOH	Sodium hydroxide
PCL	Polycaprolactone
PectX	Pectin derivative
PectX-MAL	Pectin derivative modified with maleimide functional groups
PEG	Poly(ethylene glycol)
PFA	Paraformaldehyde
TBSA	Total body surface area
TEWL	Transepidermal water loss
TIMPs	Tissue inhibitors of metalloproteinases
TSP	Trimethylsilylpropanoic acid
VEGF	Vascular endothelial growth factor
WHO	World Health Organization

CHAPTER 1 – INTRODUCTION

This chapter is based on the following publications:

1. **Luís B. Bebiano;** Flávia Castro; Ethan Y; Bruno Pereira; Rúben F. Pereira. 3D bioprinting of biofunctional tissue constructs for drug screening and tissue engineering, *In* Emerging Drug Delivery and Biomedical Engineering Technologies. CRC Press (2023), under review;
2. **Luís B. Bebiano;** Bianca N. Lourenço; Pedro L. Granja; Rúben F. Pereira. Hydrogels as dynamic networks for skin repair, *In* Hydrogels for Tissue Engineering and Regenerative Medicine: From Fundamentals to Applications (2023), under review.

1. Introduction

1.1. Context and Motivation

The skin is the outermost organ of the human body acting as the primary line of defense for internal tissues and organs. It is a complex multilayer organ that plays pivotal roles in body hemostasis by acting as a protective barrier against exogenous microorganisms, providing thermal regulation, and allowing the transmission of sensorial information. As the skin interfaces with the external environment, tissue trauma and injury are fairly common, leading to either acute or chronic wounds with different degrees of severity [2, 3].

Skin wounds represent a major healthcare problem owing to an increasing in aging population and associated health-related diseases such as diabetes. Skin wounds occurring after a traumatic or chronic episode result in disruption of the native skin structure and lead to a partial or full loss of barrier properties. Consequently, skin wounds, either chronic or traumatic, can result in long-term disability or even death [4]. In Europe, it is estimated that 1.5–2 million people suffer from acute or chronic wounds, while nearly 2.5% of the total population in the United States is affected by chronic wounds [5, 6]. Furthermore, according to the American Burn Association (ABA), about 486,000 individuals received medical treatments for burn injuries in 2016.

As a response to injury, skin triggers a series of well-orchestrated biological events at cellular and molecular levels towards the restoration of the native tissue composition, architecture and function. However, the self-healing ability of human skin is limited to small and superficial injuries [7]. Indeed, full-thickness wounds affecting deep skin layers, such as third-degree burns, do not self-regenerate and require the use of some product or therapy to stimulate the healing process. Thus, there is a critical need to develop clinically effective strategies capable of promoting the formation of functional skin, while avoiding pathological extracellular matrix (ECM) remodeling.

The selection of the most suitable therapeutic approach to promote skin repair is a multifactorial process that depends on several parameters, including the wound type (acute or chronic), lesion depth (e.g., partial-thickness, full-thickness), wound status (e.g., infected, colonized), level of exudate (e.g., dry, moderate or highly exuding wounds) and injury extension. Autologous grafts are usually the first choice for

relatively small skin injuries as they overcome potential rejection and disease transmission, which constitute issues typically associated to allografts or xenografts [8]. However, extensive lesions and deep burns often require advanced treatments, such as the application of hydrogels, antimicrobial wound dressings, ECM-derived skin substitutes, cell-laden matrices or the topical administration of growth factors [9].

In order to these innovative treatments reach the market and be largely accepted in the clinic, a series of *in vitro* and *in vivo* assays are mandatory to prove their safety, action mechanism and efficacy. For this purpose, traditional preclinical testing based on animal models and cell-based assays are the first choice. However, animal models and existing *in vitro* models based on human cells are unable to accurately replicate the anatomy, (patho)physiology and functions of human skin. Despite significant advances have been achieved in the fabrication of *in vitro* models of healthy skin, the development of biomimetic models of injured skin has been far more modest. Thus, it is of the utmost importance to develop biomimetic skin models that allow a better recapitulation of biological mechanisms underlying healthy and diseased skin morphogenesis, which is essential to improve their predictive value and reduce the failure of new products and therapies in clinical trials. Furthermore, such models also offer efficient alternatives to animal testing, which contributes to reduce animal experimentation and decrease the failure of products/therapies in clinical trials, addressing in this way the 3R's guidelines [10].

Nowadays the common approach to study the impact of burn injuries on skin wounds and test new therapies for burn wound healing relies on the use of *ex vivo* models derived from humans or animals. In a general way, skin samples are collected and then a burn injury is created by using a pre-heated tool (e.g., aluminum bar, soldering iron), which is applied to the tissue at different temperatures and for different time periods. However, the availability of human skin is limited and its *in vitro* maintenance is very limited in time. Furthermore, animal models present several disadvantages, such as high cost, time-consuming and ethical concerns. To tackle these limitations, tissue engineered skin models have emerged as powerful alternatives, as they can provide tunability of their biophysical and biochemical properties, as well as the ability to combine multiple human skin cells with engineered biomaterials towards resembling key features of native skin [11]. Regarding the fabrication of *in vitro* burn skin models, the standard approach involves the use of decellularized human skin

samples seeded and/or mixed with fibroblasts and keratinocytes to recapitulate the dermal and epidermal layers of the native skin, respectively. Nevertheless, these *in vitro* models still require the use of skin from animals to obtain the ECM used to build up the models Moreover, a standard and efficient approach to create the burn wound is still missing as the temperature and contact time are not standardized.

1.2. Objectives

The overall aim of this dissertation was to develop a biofabrication strategy comprising engineered biomaterials, human skin cells and bioprinting technology for the fabrication of an *in-vitro* tissue model recapitulating key hallmarks of skin burn wounds. More specifically, advanced design strategies for biomaterial development were implemented to bioengineer a clickable and printable bioink mimicking key features of human skin. The rheological, biophysical and biochemical properties of engineered biomaterials were optimized to support the biological function of skin cells and *in vitro* bilayered skin formation. Then, an experimental protocol to induce a burn injury in the developed bioengineered skin model was implemented, and the model was characterized using a combination of histology and confocal microscopy techniques. Finally, the bioprinting of a perfusable hydrogel construct in a customized 3D printed chip was performed as a proof-of-concept demonstration towards the generation of vascularized 3D models of skin burn wounds.

The specific objectives of the dissertation include:

- To develop a bioink exhibiting suitable rheological properties for extrusion bioprinting, and providing a skin-mimetic microenvironment to dermal fibroblasts towards stimulating *de novo* deposition of dermal tissue;
- To create a bilayer skin biomimetic model (dermis and epidermis) and characterize key features such as cell viability, cell morphology and ECM deposition;
- To induce a burn injury on the bilayer skin biomimetic model and analyze the impact of the injury regarding cell viability and morphological alterations in affected layers;
- To implement a bioprinting strategy to create advanced 3D models of skin burns on-a-chip comprising perfusable channels to mimic the vascular network of dermal region.

1.3. Thesis Outline

This thesis is structured into 5 chapters.

Chapter 1 presents a brief introduction of the research field, providing the context, motivation and relevance of the work. It also details the main goal and specific objectives of the dissertation.

Chapter 2 provides a thorough literature review of the research field discussing the major advances and bottlenecks. It focuses on human skin, burn injuries and available therapies for wound healing. Moreover, the composition and function of skin ECM, along with its biophysical and biochemical properties are also detailed. The last section is dedicated to biofabrication strategies used to create advanced models of injured and diseased skin.

Chapter 3 describes the materials and methods used in the experimental work.

Chapter 4 presents the main results obtained in the dissertation and discusses the research findings concerning the available published literature.

Chapter 5 provides the main conclusions of the research work and highlights future avenues of research.

CHAPTER 2 – STATE-OF-THE-ART

2. State-of-the-Art

2.1. Skin anatomy and physiology

The skin is the largest organ of the human body. It forms an effective barrier between the human body and the external environment, playing important functions such as protection from body dehydration and diverse forms of trauma [12].

From an anatomical point of view, the skin comprises sequential layers of epidermis, dermis and hypodermis, each one containing distinct cell populations and imparting specific properties to the skin [8].

The superficial skin layer, termed as epidermis (Figure 1), is avascular and mainly composed of keratinocytes (95%), which are responsible for the structural characteristics and impermeability of the skin [13]. It also contains non-epithelial cells such as melanocytes, Langerhans and Merkel cells that represent the remaining 5% [14]. Melanocytes are responsible for the production of melanin, which is the main pigment responsible for skin coloration. Merkel cells play a sensory role and Langerhans cells are involved in the skin immune defense [15].

The thicker skin layer, the dermis, comprises several cell types (e.g., fibroblasts, mast cells and macrophages) embedded within a complex ECM hosting a vascular network. In particular, collagen, elastin and fibronectin are prevalent in the fibrous component of the ECM, while proteoglycans and glycosaminoglycans (GAGs) such as hyaluronic acid (HA) comprise the ground substance, which provides hydration and resistance to compressive forces due to their high water binding capacity [14, 16, 17]. Fibroblasts are the predominant cell type in the dermis (Figure 1), being responsible for ECM deposition [14]. Indeed, fibroblasts play a major role in supporting skin homeostasis and responding to injury by synthesizing ECM components that maintain the tissue composition and structural organization, while directing essential cellular functions (e.g., adhesion, proliferation, migration) [15].

The hypodermis is the layer located beneath the dermis and contains a considerable amount of adipose tissue **(Figure 1)** that is well vascularized. The subcutaneous fat is a source of energy that can be further used by the body and contributes to the mechanical and the thermoregulatory properties of the skin [16, 18].

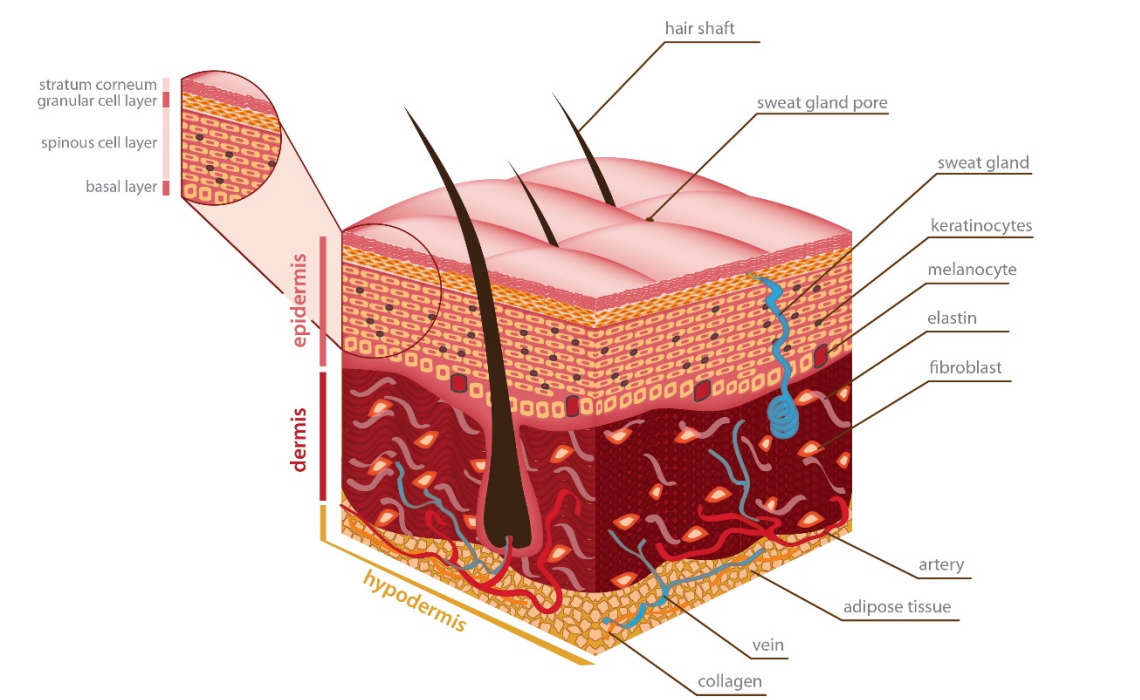

Figure 1: Representation of the major skin components and layers [1].

The skin interfaces with the external environment and, therefore, is prone to a variety of injuries, which range from surgical wounds to a deep dermal burn wound. Based on the nature of the repair process, wounds can be classified as acute or chronic wounds [13, 19].

Acute wounds are tissue injuries that heal completely with minimal scarring within the expected time frame, usually 8-12 weeks [19]. The newly formed tissue usually restores the skin anatomy and functions, though the properties of new tissue only reach ~80% of the native skin [13]. The primary causes of acute wounds include mechanical injuries due to external factors such as abrasions caused by frictional contact between the skin and hard surfaces. Other causes of acute wounds are surgery, burns and chemical injuries caused by radiation, electricity and chemicals [19].

Chronic wounds generally fail to progress through the normal stages of healing process [20], meaning that they do not heal 12 weeks post-injury. In these wounds, the normal wound healing process is altered due to repeated tissue insult or underlying pathophysiological conditions such as diabetes, persistent infections and poor primary treatment [19].

When injury occurs in the skin, a series of well-orchestrated and overlapping phases occur sequentially throughout time. Wound healing is a dynamic and highly regulated biological process **(Figure 2)** in which a variety of cellular, biochemical and matrix components act together to re-establish the integrity and function of damaged tissue through the replacement of injured ECM [19] via four sequential phases of hemostasis, inflammation, proliferation and tissue remodeling **(Table 1)** [20].

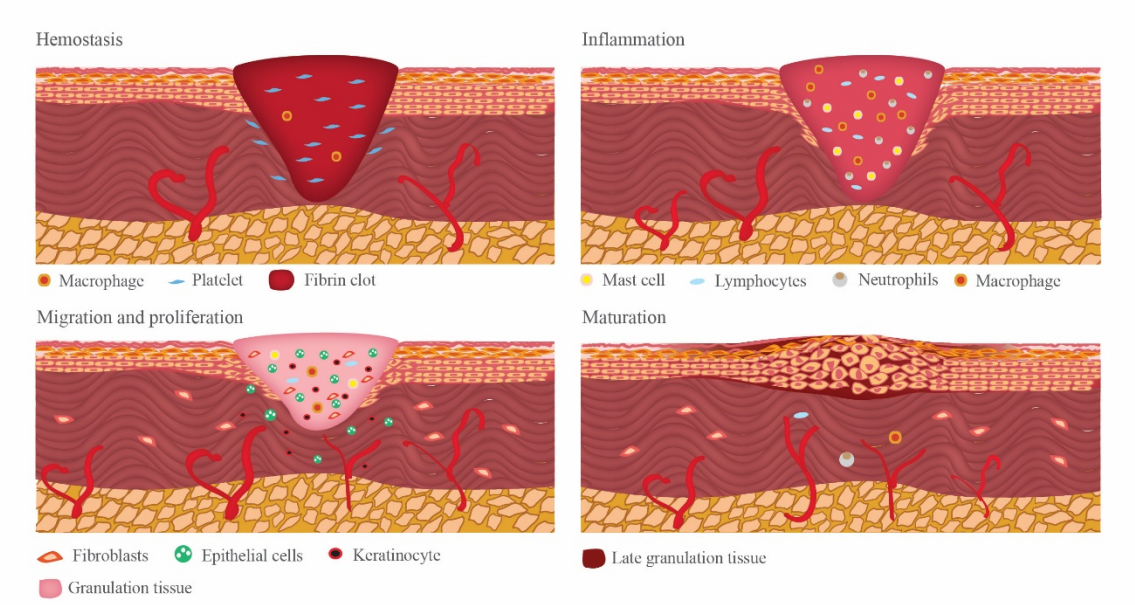

Figure 2: Phases of the wound healing process [1].

The first stage of the wound healing process consists on the formation of a provisional wound matrix, occurring immediately after injury and being completed after few hours. It begins with vascular constriction and fibrin clot formation with the ultimate goal of halting the bleeding and protecting the wound bed from foreign agents. Once the bleeding is controlled, inflammatory cells migrate into the wound (chemotaxis) and release pro-inflammatory cytokines and growth factors to promote the transition to the inflammatory phase [19, 20].

The inflammatory phase can be divided into an early phase with the neutrophil recruitment and a late phase characterized by the infiltration and differentiation of monocytes [21]. In the first days after injury, neutrophils at the wound area release mediators that amplify the inflammatory response. Furthermore, they have the ability to phagocytize bacteria and assist in the clearance of cellular debris, apoptotic cells and necrotic tissue. Approximately 3 days after injury, monocytes enter into the wound bed and differentiate into macrophages, which support the ongoing inflammatory process by

performing phagocytosis of pathogens and cell debris, as well as by secreting growth factors, chemokines and cytokines. Macrophages play multiple roles as they are involved in host defense, resolution of inflammation, removal of apoptotic cells and supporting cell proliferation and tissue regeneration after injury [20, 21]. As macrophages clear these apoptotic cells, they undergo a transition towards a reparative phenotype that stimulates fibroblasts and angiogenesis in order to promote the transition to the proliferative phase of healing process [20].

The proliferative phase aims at restoring the lost tissue at the wound surface [21]. Fibroblasts and endothelial cells are the most prominent cell types supporting the formation of granulation tissue as well as vascular network restoration [20]. The granulation tissue is formed by the proliferation of fibroblasts creating a three-dimensional ECM network of connective tissue that supports cell adhesion, proliferation and new tissue formation [21, 22]. During this initial stage of repair, type III collagen synthesized by fibroblasts is predominant in the granulation tissue [22], which is also essential for the ingrowth of new blood vessels that provide nutrition and oxygen to the growing tissue [23]. This process, known as angiogenesis, is essential for a successful wound healing. At this stage, the wound undergoes physical contraction by contractile fibroblasts, known as myofibroblasts, which apply contractile forces to close the wound edges. Keratinocytes, located at the wound periphery, migrate and proliferate into the lesion site to promote re-epithelialization [22].

Remodeling is the last phase of wound healing and occurs about 2-3 weeks after injury and can last one year or even more depending on the severity of the lesion [22]. This final stage aims to restore the native tissue structure, composition and function. This step is marked by alterations at cellular and tissue level, involving the apoptosis of myofibroblasts and the remodeling of granulation tissue to form a mature ECM mostly composed of collagen type-I [21]. The maturation phase is marked by significant changes in the ECM composition, with re-organization of collagen fibers and collagen crosslinking. Collagen III that was secreted in the proliferative phase is now replaced by thicker collagen I, imparting superior tensile strength to the tissue [22].

Table 1: Major cellular and biochemical events in the wound healing process. Adapted from [20].

Phase	Cellular and Bio-physiologic Events
Hemostasis	1. vascular constriction 2. fibrin clot formation
Inflammation	1. neutrophil infiltration 2. monocyte infiltration and differentiation to macrophage
Proliferation	1. re-epithelialization 2. angiogenesis 3. collagen synthesis 4. ECM formation
Tissue Remodeling	1. collagen remodeling 2. ECM maturation

2.2. Skin burns: impact and treatment options

Burn wounds represent a major public health problem worldwide. According to the World Health Organization (WHO), annually around 180,000 people die as a result of a burn injury, while nearly 11 million people worldwide experienced burns severe enough to require medical treatment in 2004. Moreover, according to ABA, over 486,000 individuals received medical treatment in 2016 after a burn episode. Nevertheless, the burn mortality rate has decreased in several high-income countries. However, non-fatal burns are a leading cause of morbidity due to the prolonged hospitalization time and fibrosis potentially leading to hypertrophic or keloid scars formation, which result in disfigurement and disability [24, 25].

A burn can be defined as the partial or complete disruption of the skin by thermal energy, friction, cold, radiation, chemical and electrical current. The main cause of skin burns is injury caused by heat from flames, steam, hot liquids or contact with hot objects [26]. In fact, according to the ABA, flame burns are the leading cause with 43% of the cases and scalds are in second place with 34%. Additionally, electrical and chemical burns represent only 4% and 3% of the skin wounds, respectively [24]. Moreover, besides knowing the cause of a burn injury, it is also essential to classify the wound based on the depth of the lesion **(Figure 3)** and the percentage of total body surface area (TBSA).

The depth of a burn is described in relation to the anatomical layer(s) that show damage. As a result, epidermal burns (first-degree burns) are limited to the epidermis and result in slight pain and red skin [26].

Superficial partial-thickness burns (superficial second-degree burns) are limited to the upper region of the dermis and they can heal without requiring surgical intervention. These burns are extremely painful due to the fact that the sensory nerves are intact. Deep partial thickness burns (deep second-degree burns) affect almost the entire dermis layer and, therefore, damage the pain receptors leading to a less painful burn. In addition, these injuries are characterized by both scarring and need of a surgery [26]. Full-thickness burns (third-degree burns) destroy the full dermis and usually are not painful due to damage of the nerve endings. These burns require grafting in order to protect the wound from infection and to help in skin regeneration [26]. Fourth-degree burns destroy the underlying tissue of the skin, such as muscles or bones, and can lead to the loss of the burned region [26].

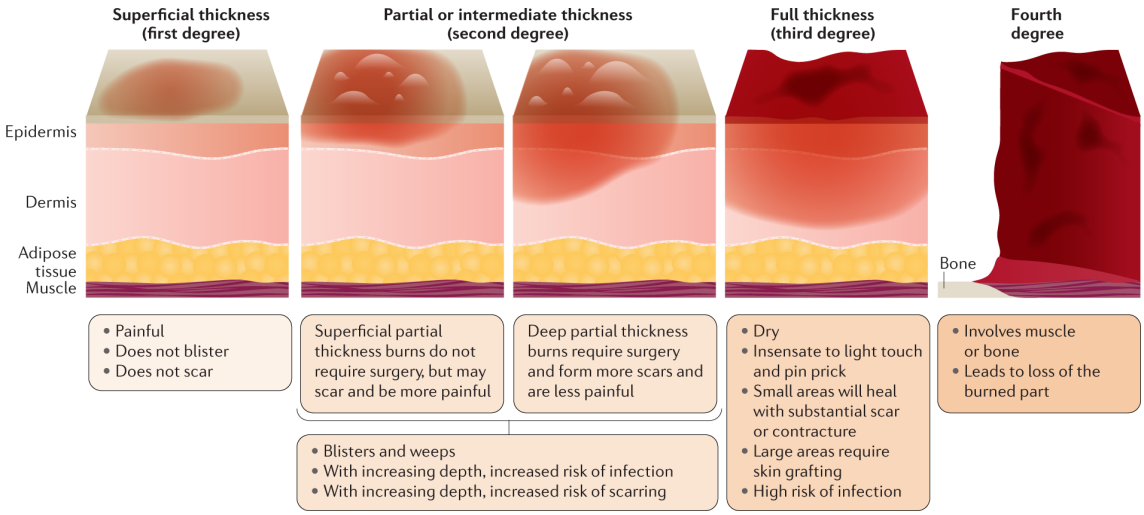

Figure 3: Classification of skin burn injuries and its main characteristics [26].

Skin burns can also be classified into minor or major burns, depending on the total body area affected. In this sense, a minor burn affects less than 10% of the TBSA, whereas major burns depend on the age of the person (over 10% of the TBSA in elderly individuals, over 20% of the TBSA in adults and over 30% of the TBSA in children) [26].

A large percentage of patients that survive to burn injuries are significantly affected in their quality of life regarding physical disability and mental health. In the most severe

burn wounds, there is a high risk of formation of a hypertrophic or keloid scar, which usually results from the persistence of an inflammatory phase, and might lead to patient morbidity, scarring, itching and microbial infections [26-28]. Indeed, hypertrophic scarring is a result of dysregulated inflammation and excessive deposition of ECM components, mainly collagen [29, 30]. Thus, there is a pathological persistence of wound healing signals or a failure of the appropriate downregulation of macrophages and myofibroblast activity, leading to skin fibrosis and the formation of hypertrophic or keloid scars [31].

The treatment of burn wounds usually involves the removal of damaged and necrotic tissue, followed by the transplantation of autologous skin grafts (autografts). However, in burns that affect large areas of the patient's body, there is a limited availability of healthy skin for harvesting and expansion. In addition, autografts also lead to pain and increase the risk of delayed healing and infection. To address these issues, several alternatives are available, including (i) skin allografts/xenografts, (ii) wound dressings and (iii) skin substitutes **(Figure 4)**. Depending on the action mechanism, these products can provide temporary or permanent wound coverage, allow pain relief, prevent fluid loss and microbial contamination, while stimulating the healing process [28, 32-34].

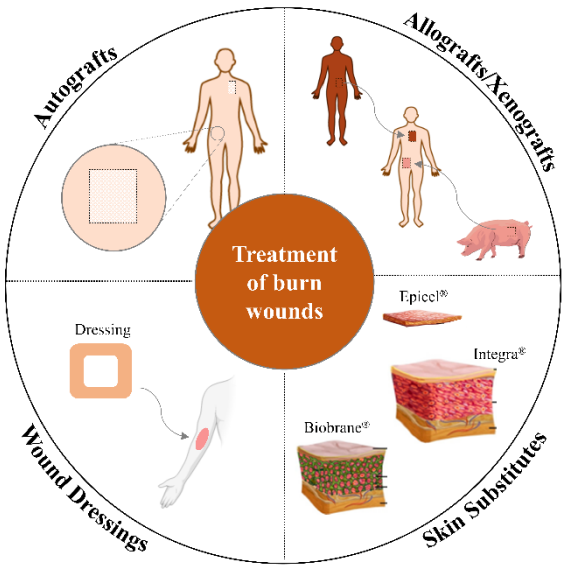

Figure 4: Schematic illustration of the main treatments of burn wounds.

Skin allografts and xenografts (mainly derived from porcine) are used to cover deep burns prior to excision, acting as temporary biological dressings. However, they present some disadvantages, such as potential risk of disease transmission, possible infection

and rejection [33]. In this regard, skin substitutes have emerged as a novel solution to cover burn wounds with promising clinical outcomes.

There are several skin substitutes currently available, which can be classified based on the number of skin layers that are going to be replaced (epidermal, dermal or both), origin (biological or synthetic) and cellular composition (cellular or acellular). Temporary skin substitutes allow for early excision while maintaining physiological wound covering until either a permanent graft is available or wound closure is achieved (in the case of partial thickness), while permanent skin substitutes integrate into the host tissue avoiding removal [33].

Epidermal Skin Substitutes

Epicel® is an autograft used to replace the outer layer of the skin and is made by isolating and expanding keratinocytes obtained from a small biopsy in sheets attached to a petrolatum gauze support. It is used for permanent wound coverage on patients with large TBSA (more than 30%) with a low risk of rejection. However, Epicel® presents some drawbacks, such as the required cell culture period (up to 3 weeks), very low shelf time (1 day) and poor outcomes with high risk of infection [35, 36].

Recell® is an autologous suspension of keratinocytes, fibroblasts, Langerhans cells and melanocytes obtained from a small skin biopsy, which is then sprayable onto the wound bed. It requires a small amount of healthy skin from the patient and, therefore, offers particular benefit to patients with burns that cover a very large TBSA. Furthermore, it reduces the healing time of the wound, and causes less pain and scarring at the donor site [37].

Dermal Skin Substitutes

Integra® is a bilayer acellular skin substitute made of bovine collagen and chondroitin-6-sulphate glycosaminoglycan as the dermal layer, and a silicone membrane as the surface layer, which provides protection against infection. The dermal layer integrates with the patient's native ECM to promote cellular ingrowth from the surrounding tissue, leading to the formation of a neo-dermis after 2-3 weeks. As the dermis starts to regenerate, the temporary outer layer is peeled away, and a very thin

autograft needs to be applied onto the wound bed. The advantages are improved wound healing time and less scar formation compared to skin grafts. However, it requires a two-step procedure, which is expensive and might lead to accumulation of exudate underneath, which increases the risk of infection [38, 39].

Dermagraft® is a bioabsorbable polyglactin mesh scaffold seeded with allogenic human neonatal fibroblasts. It produces similar results as an allograft regarding the wound infection and exudate, wound healing time and closure, and graft acceptance, being easier to be removed [38, 39]. The polyglycolic acid mesh is absorbed within 3–4 weeks, meaning that Dermagraft® should be reapplied weekly for up to 8 times [40].

Alloderm® is made of decellularized ECM (dECM) derived from a cadaveric dermis. The native ECM offers a good support for fibroblasts and endothelial cells to regenerate and proliferate to form a neo-dermis [38, 41]. Alloderm® stands out by its immunological acceptance, but has the disadvantage of being a two-step and expensive product with a high risk of disease transmission [35].

Dermoepidermal Skin Substitutes

Biobrane® consists of an inner layer of a nylon mesh bonded to an outer layer of silicon, which allows for both fibrovascular ingrowth and bacterial barrier, resembling the properties of dermis and the epidermis, respectively. The layers are embedded in porcine collagen and are widely used as a temporary skin substitute in superficial skin burns and donor sites, leading to reduced wound healing time and consequently less time of hospitalization, low pain and ready availability. However, when applied to treat partial or full-thickness skin burns, it needs to be removed before skin grafting. Moreover, there is the possibility of infection and accumulation of exudate under the substitute [38, 39].

Transcyte® consists of a bilayer model made of collagen produced by human neonatal fibroblasts cultured on a nylon mesh and an outer silicone layer to resemble both dermis and epidermis, respectively. Although the several ECM components and growth factors enhance tissue regeneration, its commonly used as a temporary wound dressing only and its very expensive. Transcyte® has the advantage of long shelf life (1.5 year), which facilitates the product availability [35, 42].

Apligraf® is composed of an epidermis made of human foreskin derived neonatal keratinocytes and a dermal layer made of neonatal fibroblasts seeded in a bovine type I collagen lattice. It is indicated to treat partial or full-thickness burns and when used for over 4 weeks of treatment it results in better wound healing than any other skin substitute currently available in the market. Moreover, when applied in combination with an autograft forms *de novo* skin that resembles the native properties with better aesthetic results. However, it has a short shelf life (5-10 days), is very expensive and there is a risk of disease transmission [35, 39].

Overall, despite there are several skin substitutes available in the market, they present critical drawbacks like limited vascularization, poor mechanical integrity, failure to integrate into the host tissue, scarring and potential immune rejection [35]. In this sense, it is of the utmost importance to develop new skin substitutes that can surpass these disadvantages and achieve better clinical outcomes. In order to develop new products that can reach the market, it is vital to better understand the pathophysiology of the burn wounds. According to the literature, the most common approach to study the effects of a burn wound is to use *ex vivo* animal models. Nevertheless, the use of animal models arises to a lot of disadvantages, namely ethical concerns and the challenge to translate novel findings from animals' models to clinical therapies for humans.

Tissue engineering has emerged as an exciting field towards the development of skin tissue models and novel products to enhance wound healing and reduce scarring [43]. In order to reach this milestone, it is vital to engineer biomimetic skin models that resemble the native biophysical and biochemical properties of human skin, providing versatile platforms for developing new therapies and screening their safety and efficacy.

2.3. 3D skin models: from traditional methods to 3D bioprinting

Bioprinting is an enabling technology used in the biofabrication field that allows the fabrication of patient-specific grafts for tissue repair and 3D *in vitro* models. The interest in bioprinting is significantly increasing as it allows the spatial arrangement of living and non-living building blocks in 3D with the ultimate goal of recreating key features of native tissues and organs at compositional, structural and functional level [44]. In addition, 3D bioprinting provides an automated and standardized fabrication

approach in comparison to manual strategies [44, 45]. Building blocks for 3D bioprinting include living cells, biomaterials and bioactive molecules. Depending on the application, building blocks can be bioprinted together or separately, allowing the fabrication of bioengineered tissues for translational applications such as tissue repair and 3D models for disease modelling and drug screening [46].

2.3.1. 3D bioprinting: principles, key elements and technologies

Several tissue engineering strategies have been proposed to develop biomimetic skin models. One of the most common strategies involves the use of the additive manufacturing technology, which comprises a group of technologies that create 3D objects through layer-by-layer deposition of materials. These technologies are assuming a pivotal role the biomedical field owing to their unique ability to generate patient-specific 3D constructs with complex shapes and controlled macro-/micro-architectures with high degree of accuracy, automation and reproducibility [47].

Bioprinting is one strategy used in biofabrication to create bioengineered 3D constructs for tissue engineering and regenerative medicine through the automated patterning and assembly of living and non-living materials [48]. In one approach, printable formulations of cells, eventually combined with biomaterials and bioactive molecules (termed as bioinks) are bioprinted into cellularized 3D constructs with structural organization and biological function. In another approach, bioprinting technologies are used for the controlled deposition of cell-free biomaterials (termed as biomaterial inks) to generate 3D scaffolds capable of guiding and instructing cells to develop into a tissue analogue.

There are multiple bioprinting technologies available, including extrusion bioprinting, light- and laser-based technologies, or inkjet bioprinting **(Figure 5)** [49]. The selection of the most suited technology depends on multiple considerations such as the resolution of bioprinted constructs, the material properties or the biological question to address. Extrusion bioprinting is the most common technology involving the pressure-driven extrusion of bioinks or biomaterial inks through a nozzle onto a substrate. Despite extrusion bioprinting allowing the deposition of multiple bioinks with distinct rheological properties, it has lower printing resolution compared to light-based technologies, such as vat photopolymerization and volumetric bioprinting [49]. These emerging technologies use light to trigger the photocrosslinking of a cell-laden hydrogel

(bioresin) and are powerful in fabricating complex 3D constructs with high resolution and intricate geometries. Indeed, in recent years there has been a growing interest in developing bioresins that meet both processing and biological requirements, which is essential to create 3D constructs with biological function [50]. Inkjet bioprinting affords the high-throughput deposition of bioink droplets through a nozzle, though it imposes some constrains to the processing of viscous bioinks [49]. Although bioprinting has been primarily explored to create grafts for tissue repair, the lack of human-relevant preclinical models for drug discovery and screening has boosted the interest in exploring bioprinting to generate biomimetic 3D *in vitro* models [46]. Such models should ideally recapitulate physiological, pathophysiological or therapeutic responses found in human body, serving as versatile platforms to study fundamental biological questions as well as to evaluate drug safety and therapeutic responses.

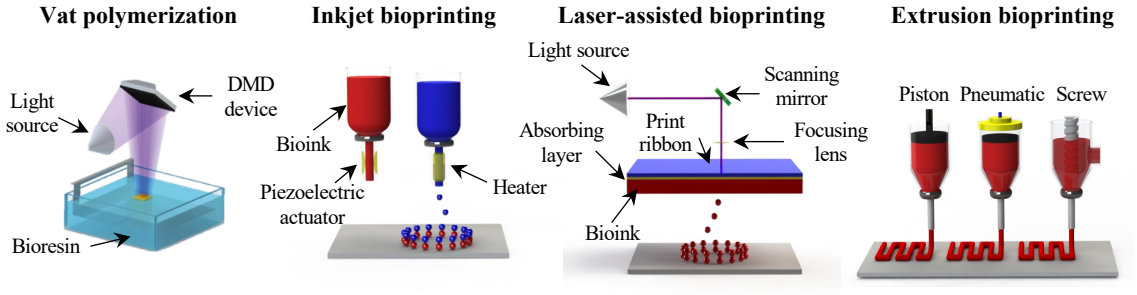

Printing resolution	+++	++	+++	+
Bioink viscosity	+	+	+++	+++
Gelation methods	Photo	Photo, ionic…	Thermal...	Photo, thermal, ionic, enzymatic...
Clinical translation	++	++	+	+++

Low (+) | High (+++)

Figure 5: Illustration of main bioprinting technologies and their characteristics. Adapted from [51].

Hydrogels are a class of crosslinked 3D polymeric networks with the ability to absorb and retain a large volume of water [52]. The high-water content contributes to their biocompatible, hydrophilic and viscoelasticity nature, resembling those features in the native ECM and making them highly attractive for wound healing applications [53]. Hydrogels present several of the desired characteristics of an ideal skin substitute as they are an effective barrier against microbial infiltration and maintain a moist environment that enhances cell migration and proliferation. Moreover, they can keep the optimal temperature onto the wound site to reduce pain, absorb of exudates and allow

the oxygen diffusion to the lesion to increase the cell activity [33, 54]. As a result of these characteristics, hydrogels are extensively used as bioinks for skin tissue engineering. The development of hydrogel bioinks is challenging due to the several requirements that need to be achieved and match the specific requirements of the bioprinting technology, including the mechanical, rheological, chemical and biological properties [55].

2.3.2. Design principles of skin-mimetic bioinks: from ECM to rheology

The ECM is a dynamic 3D network made up of proteins/glycoproteins (such as collagens, elastin, fibronectin and laminins), proteoglycans and GAG's, providing structural support for cells and tissues **(Figure 6)**. It has multiple functions such as regulating cell behavior via growth factor release, as well as the presentation of tissue/organ specific biophysical and biochemical cues to residing cells. Moreover, ECM plays key regulatory roles as it orchestrates cell signaling, functions, properties and morphology [56, 57].

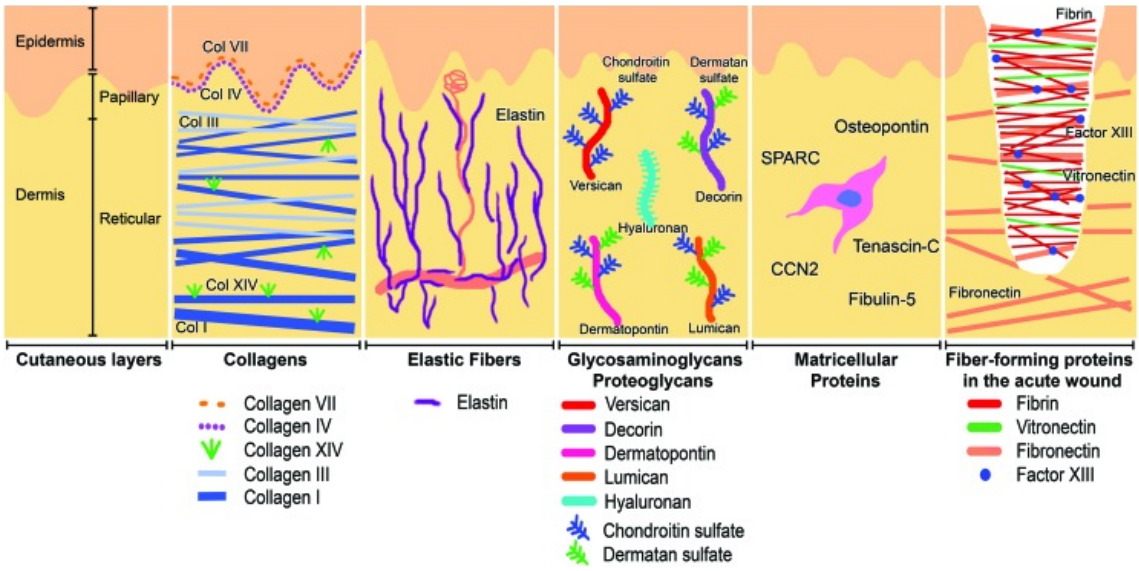

Figure 6: Components of skin ECM [58].

Collagen

Collagen is the most abundant structural protein in the ECM and possesses several functions, namely cell adhesion and migration, tissue morphogenesis and repair. It is present in the dermis as fibrillar protein, which provides tensile strength to the skin. The collagen-rich dermis is mainly composed by collagens type I and III, which make up 80-90% of the overall body collagen and are predominantly synthesized by the

fibroblasts [23, 56, 57]. Indeed, collagen type III is the most abundant in the prenatal development, while collagen type I is the dominant in the adult dermis [59].

Elastin

Elastin is a hydrophobic structural fibrillar protein assembled in a 3D network that is closely interwoven with collagen fibers. It is composed by monomers of tropoelastin, synthesized by cells such as fibroblasts and smooth muscle cells, which arrange to form the mature insoluble protein. After secretion into the intercellular space, tropoelastin spontaneously associates into larger particles through interactions between hydrophobic domains. Elastin forms a core (over 90% of the fiber structure) covered by fibrillin, a large glycoprotein that binds to elastin and it essential for the integrity of the elastic fibers. These crosslinked elastic fibers contribute to skin elasticity and its resilience to recoil after stretching [23, 59, 60].

Fibronectin

Fibronectin is a glycoprotein that possesses a vital role in cell adhesion and tissue repair. It is produced in the form of a disulfide-bonded dimer that can be broken down into subunits, of which there are three different types (I, II and III) that are repeated within each subunit. The molecules consist of differently structured sections with different functions, named as domains, which are capable to interact with the ECM proteins (e.g., collagen), GAGs, surface receptors and other fibronectin molecules. Indeed, fibronectin promotes cell binding through the RGD motif (abbreviation for the tripeptide sequence of arginine-glycine-aspartic acid), which is an integrin receptor presented in the structure of the fibronectin. Fibronectin has two distinct forms in the body known as soluble plasma fibronectin and insoluble cellular fibronectin. The plasma form is synthesized by hepatocytes and secreted into the blood to help in the homeostasis during the wound healing process. The cellular fibronectin is produced by fibroblasts, endothelial cells and others, and is assembled in a 3D fibrillar network on the cell surface and in the ECM, being responsible for maintaining the tissue architecture and regulate several cellular processes, such as adhesion, spreading, proliferation, migration and apoptosis [23, 57, 60].

Laminin

Laminin is a fibrous glycoprotein resident in the basement membrane and has an important function to form and maintain this structure. It is constituted by three disulfide-linked polypeptides, known as α, β and γ chains, which exist in various genetically distinct forms. They were first recognized as a constituent of the ECM of murine Engelbreth-Holm-Swarm (EHS) sarcoma ECM (commercially known as Matrigel). Laminins play a crucial role in cellular differentiation and migration through the tissues, and also allow cellular attachment to the underlying matrix through their integrins [57, 59, 60].

Proteoglycans

Proteoglycans are macromolecules arranged in a complex 3D structure and are composed of a protein core covalently linked to negatively charged GAGs. They present structural and biological functions, including mechanical resistance to compression and hydration of the tissues and also serve to store growth factors, cytokines and other morphogens in the ECM [60, 61]. Moreover, proteoglycans are hydrophilic molecules capable of absorbing high amounts of water, leading to the formation of a gel-like material, which keeps a proper water balance that supports the metabolic needs of the ECM [62]. One of the most predominant GAGs in the skin ECM is the HA, which is mainly produced by fibroblasts. HA increases the tissue stiffness by crosslink non-covalently with other ECM proteins (e.g., collagen) and contributes to the protection of other ECM components by absorbing shocks [63].

Growth factors

Growth factors are triggered into action by a variety of processes including wound healing and tissue remodeling [57]. For instance, the basic fibroblast growth factor (FGF-2) binds to their receptors in the presence of the proteoglycan heparin or heparan sulfate and enhances the growth of fibroblasts and endothelial cells during wound healing. Another example is the binding of vascular endothelial growth factor (VEGF) to heparan sulfate which induces the angiogenesis through regulation of the blood vessel formation and growth [62].

Matrix metalloproteinases

The breakdown and remodeling of the ECM is an essential step in the wound healing and scar formation processes [23]. The most important group of enzymes involved in the ECM degradation are the MMPs, whose action is regulated by endogenous inhibitors, known as tissue inhibitors of metalloproteinases (TIMPs) [60, 64]. MMPs are zinc-dependent containing endopeptidases that catalyze the hydrolysis of major ECM components, such as collagen, elastin, laminin and fibronectin, and contribute to the releasing of cytokines and growth factors [23, 59]. These enzymes are synthesized mainly by fibroblasts and endothelial cells [60]. MMPs can be categorized into five main subgroups based on their substrate and specificity and structural organization, including [64, 65]:

- Collagenases (MMP-1, MMP-8 and MMP-13), which degrade the fibrillar collagen type I, II, III, IV and XI;
- Gelatinases (MMP-2 and MMP-9), which degrade several ECM components, such as collagen type IV;
- Stromelysins (MMP-3, MMP-10 and MMP-11) that have similar domain arrangement as the collagenases, but do not cleave fibrillar collagen type I;
- Matrilysins (MMP-7 and MMP-26) that mainly degrade the collagen type IV;
- Membrane type (MMP-14, MMP-15 and MMP-16) that allow pro-enzyme activation by proteolytic removal of this domain and consequently conversion to an active form.

In addition to the biochemical cues described, mainly the cell-adhesion ligands and the immobilization and storage of growth factors, the ECM also provides cells with different biophysical cues, such as the structural arrangement of macromolecules and the consequent mechanical stiffness of the network and the spatiotemporal variations of these molecules, which are both interconnected and contribute to the mechanical properties of the native skin [66].

ECM structural features related with the hierarchical structure and organization of ECM fibers, such as collagen type I fibers, have a significant impact on cell activity and are directly linked to the performance and functions of tissues. Moreover, the existence of pores in the interstitial space of the ECM also creates a physically confined microenvironment that influences cell growth [66]. The native tissues exhibit properties

of both elastic and viscous materials, which induces a viscoelastic behavior. In a more detailed process, when a force is applied to living tissues, they exhibit an instantaneous solid-like elastic response. Over time, however, these forces are dissipated, and stresses are relaxed following a time-dependent liquid-like viscous behavior [67]. As mentioned above, most of the proteins that made up the ECM components contain cleavage sites that are sensitive to cell-secreted enzymes, mainly the MMPs, which induces a degradation property to the skin that is key in ECM remodeling and impacts the cell migration, proliferation and differentiation [66]. Overall, ECM provides essential biophysical and biochemical signals for regulating skin structure and function [68]. In this sense, it is fundamental to recapitulate the complexity and native properties of the ECM in order to develop human skin equivalents by providing both bulk ECM and local environmental properties to a cell **(Figure 7)**.

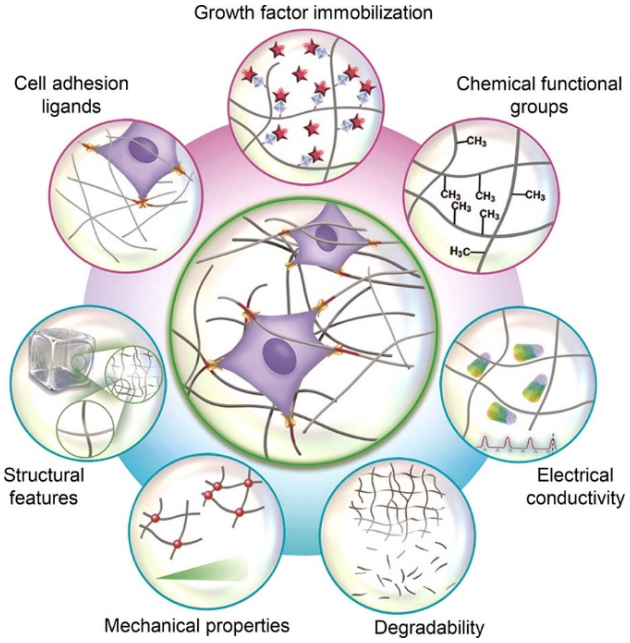

Figure 7: Biomimetic material design for engineering the 3D cell microenvironment [66].

The rational design of materials as building blocks for 3D bioprinting represents a major challenge as material properties need to fulfill not only the rheological requirements of a specific bioprinting technology, but also being compatible with cells and yield a biologically functional tissue construct. When referring to extrusion bioprinting, the bioink rheology is commonly adjusted to simultaneously allow cell mixing and extrusion bioprinting under low levels of shear stress. In this regard, there are several mechanisms to modulate the rheological properties of the bioink, such as modulating the degree of crosslinking via physical or chemical reaction, adjusting the

polymer concentration of the bioink or bleeding with sacrificial materials [69, 70]. In addition to the rheology, the material selection is another important feature in bioink design as it determines several properties of the bioprinted construct.

Decellularized ECM (dECM), which is secreted by the cells and obtained via removal of immunogenic cellular components using decellularized technologies, is commonly used as a bioink. After the decellularization process, a biomimetic ECM environment is kept, which provides a suitable microenvironment to enhance survival, maturation, differentiation, migration and proliferation of cells [71]. However, the poor mechanical properties of dECM represents a critical limitation. To overcome this issue, dECM has been mixed with other polymers or subjected to crosslinking towards increasing the mechanical properties [72]. Natural and synthetic polymers have also been used to design bioinks with different levels of control over the biophysical and biochemical cues.

Typical characteristics of natural polymers include (i) high biocompatibility, (ii) intrinsic gelation mechanisms that occur under mild conditions (e.g., thermal and ionic crosslinking), (iii) potentially metabolic processing in the human body, and (iv) eventual presence of cell-interactive motifs in the native composition, enabling cell attachment, spreading and local ECM remodeling [73]. However, natural polymers often require extensive purification steps, usually yielding hydrogels with limited mechanical performance, and are characterized by batch-to-batch variability. Despite recent developments in polymer chemistry have enabled to mitigate some of these drawbacks, synthetic polymers have been explored for applications requiring superior control over the biochemical and mechanical properties of hydrogels. These bioinert polymers offer a more controllable chemical composition and can be synthetized to exhibit specific molecular weights and functional groups, enabling the functionalization of the polymer backbone with user-defined bioactive cues (e.g., integrin-binding peptides, protease-sensitive peptides, growth factors) to engineer biomimetic building blocks whose properties can recapitulate key features of the ECM of human tissues and organs [74].

2.3.3. Bioprinted 3D models of healthy and injured skin

Skin models are usually fabricated by bioprinting through the sequential deposition of bioinks comprised of a polymer matrix and living cells specific to each skin layer.

Depending on the application, models can be bioprinted to mimic either a single or multiple skin layers [75, 76]. In the most established strategy, dermal fibroblasts are embedded within either a hydrogel precursor solution or a pre-crosslinked hydrogel and bioprinted into a dermal layer, followed by the bioprinting or seeding of keratinocytes to recreate the epidermis. Keratinocytes are usually bioprinted after the maturation of the dermal region. Following this strategy, extrusion-based 3D bioprinting was used to fabricate a full-thickness human skin model (10 x 10 mm) through the layer-by-layer deposition of a silk-gelatin bioink-laden with either human primary adult dermal fibroblasts or human keratinocytes to resemble the dermal and epidermal layer of the native skin, respectively **(Figure 8A)**. Briefly, the engineered model comprised 18 layers (10 corresponding to the dermal layer and 8 to the epidermal layer). Firstly, the dermal layer was bioprinted and then, after 3 days of culture, the epidermal layer was bioprinted on top of the dermal construct. Finally, the 3D bioprinted construct was raised to air-liquid interface (ALI) to allow differentiation of the epidermal layer. Results showed high viability of the embedded cells after the bioprinting process (up to 96%) with both fibroblasts and keratinocytes homogeneously distributed throughout the model, leading to the deposition of fibronectin and collagen type I. After 21 days of culture, keratinocytes showed extensive migration towards the pores of the 3D bioprinted construct recapitulating re-epithelialization and migration. Most importantly, immunofluorescence analysis evidenced the complete stratification and differentiation of the model resembling the structure of the native skin. However, the tensile modulus of the bioprinted construct (0.03 ± 0.005 MPa) was significantly lower than that in native skin (5.25 ± 2.0 MPa), which could be related to the differences regarding the amount of ECM components between the native skin and the *in vitro* model [77].

In recent years, remarkable progress has been made in bioprinting 3D constructs for skin modeling [78-81]. Such models have been evaluated for their ability to recapitulate key aspects of healthy and diseased skin, serving as biomimetic platforms for drug screening. The traditional bioprinting strategy involves the deposition of bioinks onto a receiving platform towards the fabrication of skin models that are subsequently cultured under static conditions using standard culture systems. Advanced strategies have been focused on generating dynamic culture systems via the fabrication of perfusable channels and integration with microfluidics. Skin-on-a-chip devices have been mostly established using traditional fabrication techniques [82], but important

advances have recently been made by exploring both 3D printing to create custom platforms for long-term culture [83] and 3D bioprinting technology to control the location of cells and materials in 3D [79]. One important consideration in bioprinted constructs for skin modelling concerns the evaluation of functional properties in order to assess their predictive value and biomimicry to the native skin. In this regard, Kim *et al* [81] created a perfusable and vascularized multilayer (epidermis, dermis, and hypodermis) healthy skin model and evaluated key characteristics such as functional markers in each skin layer and barrier function of the vascular channel. The perfusable model was generated through an integrated biofabrication strategy involving the 3D printing of a customized polycaprolactone (PCL) chamber and the bioprinting of sacrificial channels and bioinks. The model was connected to a peristaltic pump to allow dynamic culture conditions for endothelium formation and perfusion through the endothelium-lined channel to mimic vascular perfusion. Bioprinting has also been used for bioengineering 3D models of diseased skin, including hypertrophic scar [78], diabetic skin [79] and atopic dermatitis [80]. These pathophysiologically relevant models hold potential to assume a pivotal role in the screening of personalized medicine as they can be bioprinted using patients` own cells obtained from tissue biopsies and created in a reasonable time period. In a recent work, a multilayer 3D skin model recapitulating pathophysiological hallmarks of type 2 diabetes **(Figure 8B)** was established by bioprinting bioinks loaded with cells isolated from diabetic donors [79]. It was found that the diabetic skin model was able to reproduce hallmarks of diabetes such as increased insulin resistance, vascular dysfunction, delayed re-epithelialization, adipose hypertrophy, and pro-inflammatory responses **(Figure 8C)**. Moreover, by administering the drugs metformin and eicosapentaenoic acid through the vascular channel within the hypodermal region, it was possible to demonstrate the responsiveness of the model to the drugs.

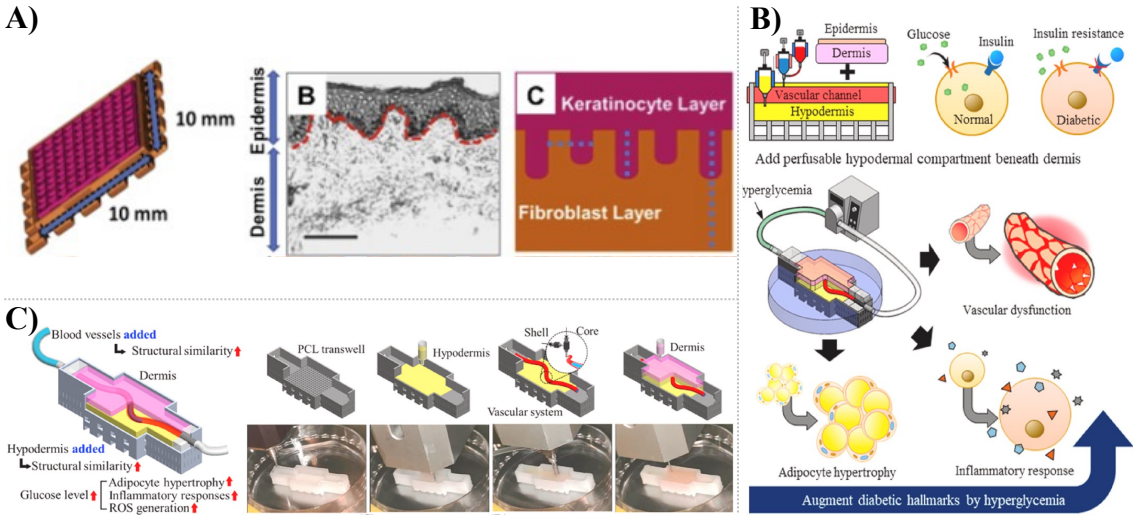

Figure 8: Bioprinted 3D models for skin modelling. A) CAD design of the dual layered skin model [77]. B) Bioprinted skin model recreating diabetic hallmarks by the inclusion of perfusable, vascularized hypodermal compartment and C) key diabetic features recapitulated by the in vitro model [79].

2.3.4. 3D skin burn models

The development of reliable 3D models of skin burn wound is very important not only to study the wound healing process, but also to test new therapies and evaluate their efficacy and safety. As stated before, burn injury is the most common cause of skin wounds worldwide. In this sense, it is of utmost importance to develop burn wound models that allow to recapitulate human burn injuries. In the literature, three main approaches have been reported to create experimental models of skin wounds: (1) *in vivo* models created in animals, (2) *ex vivo* models using explanted skin, and (3) *in vitro* skin models [84]. Furthermore, the thermal burn is the most common approach to create burn experimental models as it is the main cause of burn injury and due to the existence of several instruments capable of causing this type of burn at a controlled temperature, duration and location. In addition, these devices can be used on both small and larger animals as well as on isolated tissue *in vitro* [85].

In vivo burn wound models

The selection of the most suitable animal model for *in vivo* testing relies on several factors, such as availability, cost, easy of handling and anatomical similarity to the human skin. Although the most commonly used animal models are rodents, they present

critical anatomical differences that difficult the translational to clinical outcomes. Therefore, the pig is the most recommended animal model due to the similarity between the porcine and human skin [10, 86]. In this sense, Raut *et al* [87] used porcine models to study the variability in burn depth based on the biopsy location. For that, 24 partial thickness burns (2.5 × 2.5 cm) were created using an aluminum bar heated in a water bath to 80 ºC and applied for 20 seconds on the back of anesthetized pigs. Following the burning procedure, the necrotic epidermis was removed from the wound surface of one of the animals by scraping the burn (debrided burn). Then, 1 hour after injury, five full-thickness 4 mm punch (four corners and center of the burns) were obtained from both pigs. Results showed that the non-debrided burns were 0.24 mm deeper than debrided burns **(Figure 9A)**, and that the partial-thickness contact burn was highly reliable with very little variation in burn depth.

Ex vivo burn wound models

The *ex vivo* models present some advantages, including the more controlled experimental conditions, fewer ethical concerns compared to *in vivo* studies, and a closer representation of the native skin compared to *in vitro* methods [88]. Therefore, several studies have been conducted using skin explants. In one example, a hot plate at 85 ± 1 ºC was placed in direct contact with samples from porcine skin for 4, 7 or 10 seconds to simulate different degrees of burns. It was found that the skin burned for only 4 seconds already induced significant tissue damage as transepidermal water loss (TEWL) showed values over 30.9 ± 1.0 g/h/m^2. In fact, tape-stripped skin, which is a well-known technique for damaging the skin barrier, only reached a critical TEWL state (38.5 ± 3.6 g/h/m^2) after the removal of 30 tapes (very healthy skin is considered under 10 tapes), showing the efficiency of the experimental approach. Moreover, increasing the time of the skin in contact with the hot plate, a first-degree, a second-degree and a deep second-degree burn injury was obtained, respectively [89].

Besides studying and optimizing the creation of the burn, *ex vivo* models have also been used to evaluate the antimicrobial efficacy of topical formulations. In this regard, Puthia *et al* [88] used an electric soldering iron preheated for 10 minutes to obtain a temperature of 368 ºC and then placed against the defrosted skin of minipigs and held with a uniform pressure for 15 seconds to create burn wounds. Hematoxylin/Eosin (H&E) stained sections of the wound showed that the freeze-thawing process did not

present any adverse effect and was comparable to the fresh porcine skin tissue **(Figure 9B)**. In order to study the antimicrobial activity of topical formulations, wounds were infected with either Gram-positive *Staphylococcus aureus* or Gram-negative *Pseudomonas aeruginosa* and, two hours after the infection, a topical gel (Prontosan) and a water-soluble antibiotic (Levofloxacin) were applied topically on the wounds. Prontosan treatment reduced both *S. aureus* and *P. aeruginosa*, while Levofloxacin reduced only *S. aureus* in the wound tissue. Moreover, Levofloxacin treatment showed a dose-dependent response, demonstrating the sensitivity of the model. Overall, these results show that the burning procedure produced burn wounds with reproducible size, depth and surface, holding potential to be used as a tool to study the penetrating properties of both pathogens and drugs into soft tissues. However, as it is a frozen porcine skin model, it has no active immune system in the tissue and, therefore, it cannot replicate the complex *in vivo* wound healing process.

A multitude of *ex vivo* thermal burn models has been reported by using fresh human skin samples. In this regard, Ulrich *et al* [90] developed a burn wound model by applying a cooper device (2 × 10 mm) attached to a soldering iron at 95 ºC for 10 seconds without exerting pressure to *ex vivo* human skin samples from five healthy donors. During culture, re-epithelialization and fibroblast migration into the wound took place from the surrounding tissue. In addition, the newly formed epidermis was accompanied by restoration of the basement membrane as shown by the presence of collagen type IV and laminin. However, reepithelialization of the wound model occurred much slower than *in vivo* (≈50 mm instead of 150–300 mm/day).

In a recent study, Kotzbeck *et al* [91] used fresh abdominal skin explants from eight healthy female donors and contact burn injuries were created by application of heated metal blocks (5 × 5 cm, 100 ºC) onto the samples for 10 seconds. Histology results showed that the burn-induced tissue damage corresponded to a partial-thickness burn, with complete disintegration of the epidermis, and partial denaturation of the dermis in comparison to the unburned skin . Moreover, expression of factors involved in tissue regeneration and inflammation significantly increased after the burn injury. In this sense, this *ex vivo* human skin model is suitable to study the local and immediate mechanisms involved in the wound healing process of the skin after a burn injury. However, this *ex vivo* approach is limited by the lack of a blood circulation in the explanted skin and the inflammatory responses analyzed only reflect the local responses

of skin-resident immune cells, such as the platelets, due to the fact that the neutrophils and monocytes cannot infiltrate to the site of the burn injury.

Similarly, human skin tissue discarded from surgeries of six healthy donors was exposed to either pre-heated steel (100 ºC) for 30s or a precision flame burner (300 ºC) for 15s. On one hand, the flame burns instantly caused deep and stable damage to the subcutaneous tissue, which did not significantly change for 7 days. On the other hand, contact burns inflicted tissue damage that was initially superficial but then expanded deeper into the adipose tissue. On the whole, the investigators concluded that the type of burns and their thermal characteristics, like heat source and duration, are crucial to the initial decision-making in primary care [92].

However, animal models present critical disadvantages, including the different anatomical and physiological properties of rodents in comparison to the humans, the waste of several animal tissues if not used immediately and, for example, despite pigs having a skin similar to the human, they are expensive and difficult to handle. Therefore, it is difficult to directly translate novel outcomes from animal models to the clinical situation [91, 93]. In addition, most *ex vivo* models lack a full range of host responses and experiments need to be carried out for shorter time periods in comparison to *in vivo* models [88, 91].

In vitro burn wound models

Tissue engineering has emerged as a promising approach to develop *in vitro* skin models to surpass the current limitations of *in vivo* and *ex vivo* models. Although *in vitro* models cannot resemble all the properties and functions of native skin (e.g., epidermis, dermis, lymphatic and immune system), they allow to develop models with superior control of their properties, allowing to perform more controlled studies aiming at addressing a specific research question. Moreover, *in vitro* models possess high standardization with an easy implementation into standard cell culture systems. In this sense, *in vitro* models have recently been used to study the burn wound healing [94].

Groeber-Becker *et al* [94] developed an *in vitro* 3D epidermal burn model using primary human epidermal keratinocytes (5×10^5 cells in 500 µL medium) cultured for 12 days before burning. On day 12, a thermal burn was created at the center of the model by applying a metal rod (6 mm diameter) pre-heated to 83 ºC on the model for 7

seconds without the use of further pressure **(Figure 9C)**. The injury led to a local reduction of cell viability in comparison to unburned models, showing the effectiveness of the procedure. After 14 days post-injury, keratinocytes started to ingrow and close the burn wound and a new epidermis was formed as well, pushing the remaining dead tissue in the wound area off the cell culture membrane. In fact, the wound size decreased from 25% to 5% of the model area. As a whole, this model allows a deeper and more specific study of the consequences of a thermal burn on the epidermal wound healing.

In a novel approach, Cuttle and colleagues [93] developed a 3D human skin equivalent (HSE) model using dermis derived from abdominoplasty/breast surgery, primary keratinocytes and fibroblasts. In detail, human surgical discarded skin (2 cm × 2 cm) was dissected and the epidermis and dermis were separated into small pieces to create a de-cellularized and de-epidermized dermis (DED). Afterwards, DED was seeded with a cell suspension containing keratinocytes (7.2×10^4 cells/mL) and fibroblasts (3.6×10^5 cells/mL), creating the HSE. After 10 days of culture, a contact burn was created with different burn depths (60 ºC for 20 s, 80 ºC for 20 s, 90 ºC for 30 s) using a modified soldering iron. Results demonstrated that native skin showed a clear burn area after 7 days post-injury in all conditions, while in the HSE only the burn wound area at 90 ºC was visible on day 7. Moreover, the HSEs showed evidence of healing, with formation of a neo-epidermis and expression of markers for proliferation, differentiation and wound healing after 7 days, whereas the *ex vivo* native skin did not **(Figure 9D)**. However, it is important to highlight that the process implemented to create the HSE was unclear as the authors do not provide a clear explanation about how a cell suspension of containing DED, fibroblasts and keratinocytes can lead to the formation of a skin model resembling the native skin.

Based on the literature analysis, the gold-standard approach to study burn wounds are either *in vivo* animal models or *ex vivo* animal samples. However, as aforementioned, the use of animal models has several drawbacks, such as the physiological and anatomical differences compared to the human skin, as well as the high costs and ethical concerns. Furthermore, experiments on animal models require the creation of several burns using a high number of animals, which is in contrast with the 3R`s principles aiming at the “Reduction, Refinement and Replacement” of animal testing. Another common approach is to use *ex vivo* human samples, which surpass the

limitations regarding the use of animal models. However, these samples present high variability from donors, and their availability and maintenance under *in vitro* culture are very limited. Besides these limitations, a standardized experimental approach to create the burn wound is still missing as there are several studies reporting the use of different tools and their application at different temperatures and for varying time periods to induce the wound. Therefore, considering all the critical disadvantages of the current models, it is of utmost importance to develop an *in vitro* 3D skin biomimetic model that resembles the epidermis and dermis of the native skin and is amenable to generation of burn wounds. Such a model would provide a versatile and controllable platform to understand the impact of burn wound in the skin and test new treatments for burn wounds.

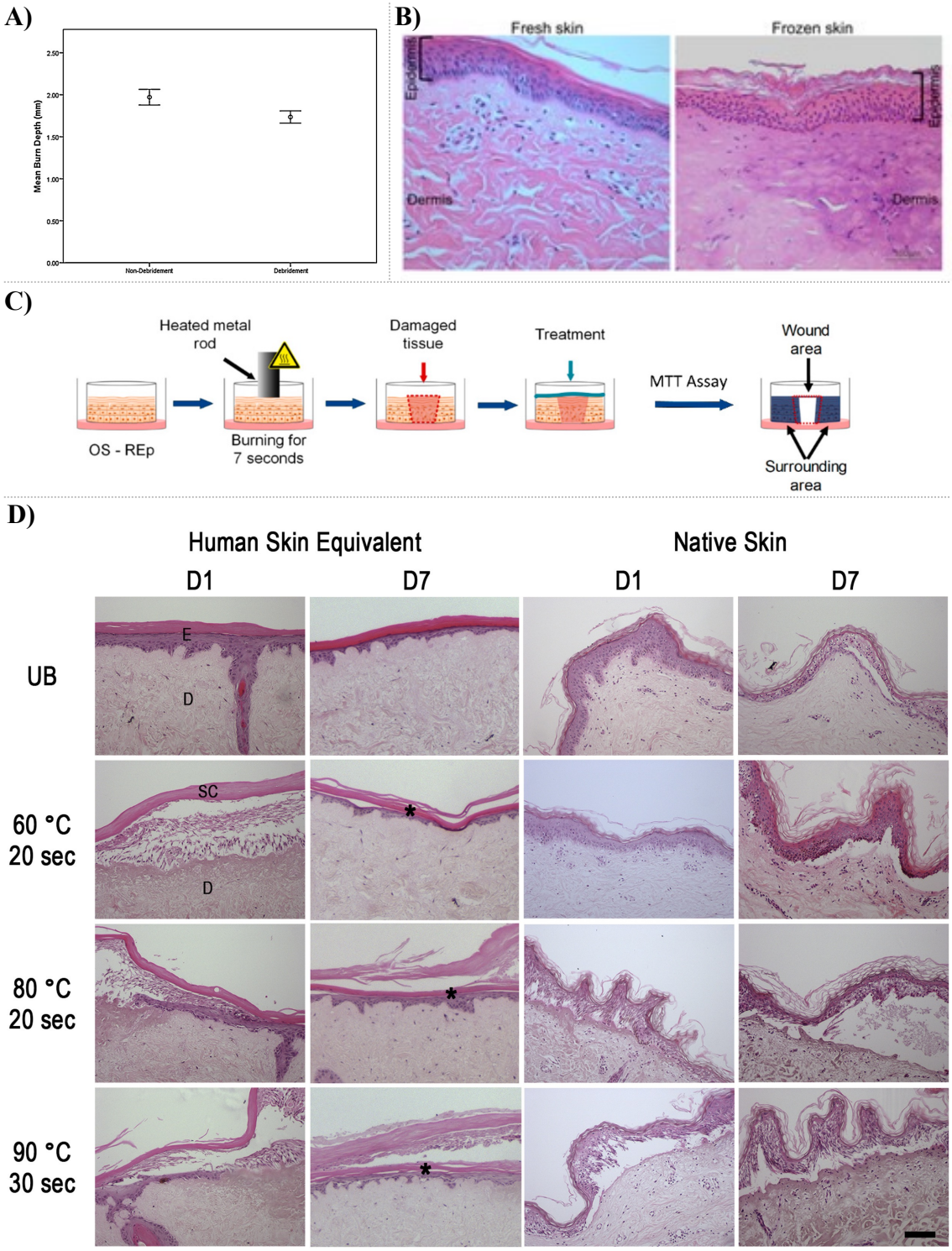

Figure 9: Bioengineered skin burn models. A) Comparison of burns from non-debrided and debrided pigs [87]. B) H&E staining comparing freshly excised and freeze-thawed porcine skin tissue [88]. C) Schematic illustration of the experimental method to generate a burn wound [94]. D) H&E staining of human skin equivalent (HSE) and native skin at days 1 and 7 after the creation of burn wounds with different depths [93].

CHAPTER 3 – MATERIALS AND METHODS

3. Materials and Methods

3.1. Synthesis of maleimide modified derivative of pectin

For the synthesis of a pectin derivative (PectX) modified with maleimide functional groups (PectX-MAL)[1], 1-(2-Aminoethyl)maleimide hydrochloride (maleimide, Sigma) was introduced into the polymer backbone by amidation of the carboxyl groups using 4-(4,6-Dimethoxy-1,3,5-triazin-2-yl)-4-methylmorpholinium chloride (DMTMM, Sigma) as the coupling reagent. PectX (1% w/v) was dissolved in ultrapure water, then DMTMM was added (5.5 mM) to activate the carboxyl groups and left to react for 30 minutes. Afterwards, 1-(2-Aminoethyl)maleimide hydrochloride (Sigma) was added (0.6 mM) and the mixture was stirred for 24 hours. The reaction product was dialyzed (MWCO 3500, Spectrum Labs) against decreasing concentrations of sodium chloride (NaCl) for 3 days. Finally, the pH of the polymer solution was adjusted to 7.00 with 0.1 M sodium hydroxide (NaOH), filtered (0.20 μm) and the PectX-MAL was recovered by lyophilization. Maleimide modification was assessed using ^{1}H NMR by dissolving the polymer in deuterium oxide (D_2O) and trimethylsilylpropanoic acid (TSP) at 0.05M was added as an internal standard. Spectra was acquired on a 400 MHz Bruker spectrometer and analyzed using MestReNova software. To calculate the modification degree of the PectX-MAL, integrals corresponding to the peaks of the proton in native polymer backbone (4 ppm) and the protons of the carbon double bond in maleimide (6.8-6.9 ppm) were selected, and the degree of substitution calculated according to the Equation (1):

$$Degree\ of\ substitutiion\ (\%) = \frac{\frac{\int Maleimide\ peak}{2}}{\int Maleimide\ peak + \int Proton\ peak} \times 100$$

3.2. Cells and cell culture maintenance

Dermal fibroblasts isolated from human neonatal foreskin (hNDFs) samples (passages 6-8) and immortalized human keratinocytes (HaCaT) were cultured

[1]PectX means a polymer derivative of pectin obtained by specific purification and chemical modification reactions. As a patent request is under preparation, the exact chemical composition and fabrication methods are confidential. Thus, in the scope of this dissertation, the polymer is referred as PectX.

in Dulbecco's Modified Eagle Medium (DMEM) high glucose (Lonza), supplemented with 10% (v/v) fetal bovine serum (FBS) (Gibco) and 1% (v/v) of both penicillin/streptomycin and Amphotericin B. Cells were cultured in 5% CO_2 at 37 ºC in tissue cultured polystyrene flasks. At specific time periods, cells were trypsinized when reaching 80% confluence using 0.05% (w/v) trypsin/ethylenediaminetetraacetic acid (EDTA) solution and centrifuged at 1200 rpm for 5 min to obtain the cell pellet or for subsequent cell expansion.

3.3. Hydrogel fabrication and bioink crosslinking

Hydrogels were prepared by the sequential mixture of individual components at the desired concentrations. First, PectX-MAL (final concentrations of 2% or 3% w/v) was dissolved in the Hank's Balanced Salt Solution (HBSS, Gibco) buffer. Then, the cell-adhesive peptide ligand CGGGGRGDSP (final concentration of 2 mM, GenScript) was added to the solution and reacted for 20 minutes to allow peptide tethering to maleimide groups. Afterwards, calcium chloride dihydrate ($CaCl_2{\cdot}2H_2O$) (147.02 g/mol, Acros Organics) solution (final concentration of 8-12 mM) was added to the polymer under vigorous vortex agitation for a better homogenization and left to crosslinking for 1 hour (8% v/v of the total bioink volume). After ionic crosslinking, hNDFs were gently added to the solution ($10{\times}10^6$ cells/mL, 8% v/v of the final bioink volume). Finally, desired volume of the crosslinker was added to achieve a final concentration of 0.125 or 0.5 mM. To promote chemical crosslinking, three different crosslinkers were used: (i) non-degradable dithiothreitol (DTT, Sigma), as well as the MMP-degradable peptides CGPQG↓IWGQC (termed as MMP, GenScript) and CVPMS↓MRGGC (termed as MMP+, GenScript), where the arrow indicates the enzymatically cleavable site. According to literature, the peptide sequence CVPMS↓MRGGC is more degradable than CGPQG↓IWGQC [95]. Immediately after the crosslinker addition, the polymer solution was mixed, casted (25 μL) onto a SigmaCote-treated glass slide, and left for 20 minutes to allow the thiol-Michael addition reaction to proceed. Bioinks were prepared using the same procedure, expect that instead of mixing the chemical crosslinker with the bioink prior bioprinting, it was added only after the bioprinting process to trigger chemical crosslinking and allow stabilization of bioprinted construct.

3.4. Rheological characterization

The rheological behavior of bioinks was analyzed in a Kinexus Pro rheometer (Malvern) at 25 °C. The rotational shear viscosity measurements were performed using a shear ramp test (1-1000 s^{-1}, 2 minutes) after applying one loading cycle with 2 minutes interval before the rheological data acquisition. The gelation kinetics of bioinks was determined by measuring the evolution of both storage (G') and loss (G'') modulus at a strain of 1% and frequency of 0.1 Hz.

3.5. Hydrogel viscoelasticity

To characterize the viscoelastic properties, hydrogels were incubated in DMEM at 37 °C for 24 hours before testing. Then, 4 mm diameter samples were obtained and analyzed in a Kinexus Pro rheometer (Malvern). Samples were compressed at 20% of their initial height and strain amplitude sweeps were conducted from 0.1 to 100% at 0.1 Hz, while frequency sweeps were carried out from 0.01 to 10 Hz at 1% strain (within the linear viscoelastic region).

3.6. Cell behavior within 3D hydrogels

At predetermined time periods (days 1, 7 and 14), cell-laden hydrogels were collected and characterized for their metabolic activity, cell viability, cell morphology and ECM deposition.

The metabolic activity of the cells embedded within hydrogels was determined by the resazurin assay. Hydrogels were incubated in DMEM containing 20% (v/v) resazurin sodium salt (Sigma) for 2 h at 37 °C, and the fluorescence was measured using a microplate reader (Synergy MX, BioTek) at 530 nm (excitation) and 590 nm (emission).

The cell viability was analyzed by Live/Dead assay. Briefly, cell-laden hydrogels were incubated in phenol red-free DMEM media containing 1.99 µL calcein in 1 mL DMEM and 2.5 µL ethidium homodimer in 1 mL DMEM for 30 minutes and, finally, washed with HBSS before analysis. Cell-laden hydrogels were imaged on a confocal laser scanning microscope (CLSM, Leica TCS-SP5 AOBS, Leica Microsystems).

For immunofluorescence analyses, cell-laden hydrogels were fixed using 4% (v/v) paraformaldehyde (PFA, Electron Microscopy Sciences) in HBSS for 20 minutes,

washed and stored at 4 °C in HBSS. Cell morphology was visualized by immunofluorescence staining of F-actin (phalloidin/Alexa Fluor 488) and nuclei (Hoechst) overnight at 4 °C. Then, samples were rinsed with HBSS and imaged on a confocal laser scanning microscope (CLSM, Leica TCS-SP5 AOBS, Leica Microsystems). The ECM deposition was analyzed by immunofluorescence staining of fibronectin. Samples were permeabilized with Triton X-100 (0.1% w/v, 10 minutes) in HBSS, washed and incubated in blocking solution (1% w/v bovine serum albumin, BSA) for 30 minutes. Then, samples were incubated overnight at 4 °C with phalloidin/Alexa Fluor 488, rabbit anti-fibronectin antibody (1:400, F3648, Sigma-Aldrich) and nuclei (Hoechst). Afterward, samples were rinsed with HBSS and incubated for 45 minutes with Alexa Fluor 594 goat anti-rabbit secondary antibody (Molecular Probes-Invitrogen). Finally, samples were rinsed with HBSS and imaged on a confocal laser scanning microscope (CLSM, Leica TCS-SP5 AOBS, Leica Microsystems).

3.7. Bioprinting of 3D cell-laden hydrogels

Hydrogels were bioprinted using the Regemat 3D V1 system (Regemat 3D, Spain). For that, the bioink was loaded in a 3 mL sterile syringe (Nordson EFD) and bioprinted into 3D constructs (10 × 10 × 1.23 mm^3, 3 mm/s printing speed, 0.8 mm/s nozzle flow speed, 0.41 mm smooth nozzle diameter). Then, the scaffold was chemically crosslinked and, finally, incubated in DMEM at 37 °C. At day 1 post-printing, cell viability was evaluated by Live/Dead assay as previously described.

3.8. Fabrication of *in vitro* skin models and burn wound injury

Two skin models were created, including (1) a model of the dermis comprising the dermal layer and (2) a bilayer model consisting of both epidermal and dermal layers. For the dermis model, cell-laden hydrogels were prepared as described and manually casted onto a 12-well Transwell inserts (ThermoFisher Scientific). The model was cultured for 28 days before analysis. For the fabrication of the bilayer skin model, the same procedure was applied to create the dermal layer, but the dermis was cultured for 7 days. After this time period, HaCaT cells were seeded on top of the dermis at different densities (1×10^6 cells, 1.5×10^6 cells, 2×10^6 cells and 2.5×10^6 cells) to study its impact on epidermis formation. To develop the bilayer skin burn model, HaCaT cells were seeded at 2×10^6 cells in 250 µL of DMEM to allow cell attachment. After 24 hours,

additional culture media was added, and the model was cultured under submerged conditions for 1 week. Then, the model was raised to the ALI condition for 2 weeks. In both models, the culture medium was changed every 2-3 days. To create the burn wound, a stainless-steel rod with 5 mm diameter at 65 °C was placed in contact with the model for 120 seconds with a uniform pressure. Samples which were not subjected to the burn process were used as controls. After either 1 or 7 days, live/dead assay and histology were performed to assess the effectiveness of the approach in inducing a burn wound.

3.9. Histological analysis of skin burn wound models

Skin burn wound models were rinsed with HBSS, fixed in 4% (v/v) PFA in HBSS for 40 minutes and extensively washed with HBSS. Then, samples were embedded in paraffin, sectioned onto 3 μm slides and representative sections were stained for H&E and Masson's Trichrome using routine protocols. The sections were mounted on coverslips and observed with an optical microscope.

3.10. Bioprinting a 3D model burn skin wound on-a-chip

As a proof-of-concept of the fabrication of a 3D skin burn wound model on-a-chip, a printing strategy comprising the deposition of a sacrificial biomaterial ink and casting of a cell-laden hydrogel was implemented.

First, a gasket made of Kolliphor® P407 (Sigma), also known as Pluronic F127, was printed using the Regemat 3D V1 system (Regemat 3D, Spain). Specifically, the biomaterial ink (27.5%) was loaded into a 3 mL sterile syringe (Nordson EFD) and printed into a mold square box (8 × 8 × 4.1 mm^3, 3 mm/s printing speed, 2.5 mm/s nozzle flow speed, 0.41 mm stainless steel nozzle diameter). Then, the Pluronic F127 mold was placed in an oven for 30 minutes at 37 °C to increase the stiffness. Then, PectX-MAL containing fibroblasts cells was manually casted onto the mold, followed by the embedded bioprinting of Pluronic F127 biomaterial ink to create a sacrificial channel. The sacrificial channel was printed using the Nordson EFD PRO4 printer coupled with a vision system to define the nozzle positioning and printing path. For that, Pluronic F127 was loaded in 3 mL sterile syringe (Nordson EFD) and printed into a channel (0.5 mm/s printing speed, 0.9 bar nozzle flow speed, 0.51 mm stainless steel nozzle diameter). Afterwards, chemically crosslinking was performed using DTT (0.125

mM, 20 minutes) for the stabilization of the cell-laden hydrogel. Finally, the hydrogel was placed on ice (4 ºC) for 2 minutes to remove the sacrificial ink to leave a perfusable channel. To demonstrate the perfusion of the channel within the 3D hydrogel, Fluorescein sodium salt (Sigma) was injected into the channel and the hydrogel was subsequently incubated in culture medium.

3.11. Statistical analysis

Statistical analyses were performed using GraphPad Prism 8.0 software and the results presented as the mean ± standard deviation. For each study, at least two independent experiments were performed. Mann–Whitney test was applied for single comparisons with 95% confidence interval and differences were considered statistically significant for *p*-values lower than 0.05.

CHAPTER 4 – RESULTS AND DISCUSSION

4. Results and Discussion

4.1. Design and synthesis of click crosslinked hydrogels

Natural polymers are extensively used in the biomedical applications as they present several advantages when compared to synthetic ones, including the wide range of biophysical and biochemical cues, biocompatibility and, in some cases, the similarity to the native ECM components. Recently, pectin has emerged as an attractive biomaterial for tissue engineering applications due to its high biocompatibility, biodegradability, and tuneability of its rheological behavior and mechanical properties via ionic crosslinking [96, 97].

Pectin tends to dissolve under physiological conditions and, therefore, physical and chemical crosslinking mechanisms are required to produce stable pectin-based hydrogels. Crosslinking leads to the formation of a 3D hydrogel that prevents network dissolution, though special attention should be given to the stability of each crosslink in physiological conditions. One of the most explored crosslinking mechanisms of pectin-based hydrogels is ionic gelation, which explores the native ability of pectin to form physically crosslinked hydrogels through ionic interaction of carboxylic groups in pectin backbone and divalent or trivalent ions (e.g., $CaCl_2$) in solution. Ionic crosslinking allows for easy modulation of the crosslinking degree of hydrogels and their rheological behavior by simply tuning the concentration of divalent ions in solution and/or the polymer content. Furthermore, the chemical structure of the pectin backbone is amenable to chemical modification towards the introduction of several functional groups (e.g., maleimide, methacrylate or norbornene groups), which allow the use of additional crosslinking strategies (e.g., thiol-Michael addition click reaction, photocrosslinking) for hydrogel crosslinking. Additionally, the absence of cell-adhesion and cell-degradable sites in polymer backbone allows to modulate its cell interaction, for example, via incorporation or functionalization with cell-adhesive peptides and cell-degradable crosslinkers [96, 98, 99].

Herein, a novel single-polymer bioink was developed using a pectin derivative with tunable mechanical and rheological properties that can be functionalized with relevant peptides to engineer pathophysiological relevant models of skin burn wounds. Specifically, maleimide-functionalized pectin (PectX-MAL) was used as a base polymer for the fabrication of cell-laden hydrogels through a sequential dual-crosslinking

mechanism based on both ionic crosslinking and thiol-Michael addition click reaction. PectX was reacted with DMTMM for 30 minutes to allow amidation of carboxyl groups in the polymer backbone, followed by the addition of maleimide groups to functionalize the polymer backbone **(Figure 10A)**. In the ^{1}H NMR spectra, the appearance of new characteristic peaks of maleimide group at 6.8-6.9 ppm corresponding to the protons in the double bond of the maleimide group, originally absent in the pure polymer, demonstrate the success of polymer functionalization **(Figure 10B)**. The degree of modification was calculated to be 7.6% through ^{1}H NMR analysis by comparing the integral values corresponding to maleimide groups and native protons in the polymer backbone (4 ppm).

To create hydrogels, a bioinspired strategy was implemented based on the use of a thiolated cell-adhesive peptide ligand, calcium ions, a biscysteine crosslinker and human skin cells **(Figure 10C)**. These components were selected to recreate key ECM features serving specific purposes on bioink design and hydrogel properties: i) tethering of the cell-adhesive peptide (CGGGGRGDSP) to provide anchorage sites to the otherwise non-adhesive cell hydrogel; ii) calcium ions to tune bioink rheology and impart viscoelastic properties to the gel network through the formation of physical crosslinks via reaction with carboxylic groups in the PectX backbone; iii) biscysteine crosslinker to allow the formation of chemical crosslinks in the hydrogel by thiol-Michael addition click reaction with the maleimide groups, which are essential to stabilize the gel network and eventually afford cell-mediated crosslinker degradation (in case of degradable peptide crosslinkers); iv) primary human fibroblasts that constitute the cellular component, given their pivotal role in skin ECM remodeling. This design strategy allows the development of hydrogels mimicking key features of skin ECM, while controlling the rheological, biophysical and biochemical properties in an independent manner.

3D bioprinting is an additive manufacturing technique that allows to create complex cell-laden constructs in a cost-effective and reproducible manner. Bioinks used in extrusion bioprinting need to fulfill several requirements, including proper mechanical, rheological and biological characteristics. Ideally, these properties would lead to the formation of tissue constructs with adequate cell-instructive properties and high shape fidelity, which are essential for tissue morphogenesis. However, it is vital to find a proper balance between the rheological properties (e.g., viscosity, filament

stability, shape fidelity) and bioprinting conditions in order to preserve cell viability and function [55, 100]. The novel bioink presented in this work allows to explore a versatility of ionic crosslinking to expand the bioprinting strategies for bioink processing. Notably, the ability of PectX-MAL to form physical hydrogels in the presence of divalent ions was explored as an efficient strategy to adjust the bioink rheology. On one hand, at lower $CaCl_2$ concentration (8-10 mM), the crosslinking degree of the bioink is low enough to support the printing of sacrificial biomaterial inks in 3D, which is useful to create perfusable channels **(Figure 10D, left)**. On the other hand, at a higher $CaCl_2$ concentration (12mM), the bioink has a higher and suitable crosslinking degree to allow the bioprinting of 3D hydrogels with controlled pore size and high shape fidelity **(Figure 10D, right)**. Upon bioprinting, the ionically-crosslinked hydrogel is subsequently crosslinked via thiol-Michael addition click reaction to modulate the mechanical properties and tune the degradation of hydrogels by selecting the type of crosslinker agent. Despite the material used in this experimental work is new, the use of maleimide groups to create clickable hydrogels for regenerative medicine applications has been extensively reported in the literature due to their higher reactivity towards thiols when compared to other groups (e.g., acrylates, methacrylates), which allow to significantly reduce the crosslinking time. For instance, García *et al* [101] reported outstanding results for the delivery of therapeutic proteins for cardiac repair and pancreatic islet delivery and engraftment using poly(ethylene glycol) (PEG) hydrogels crosslinked using maleimide reactive groups.

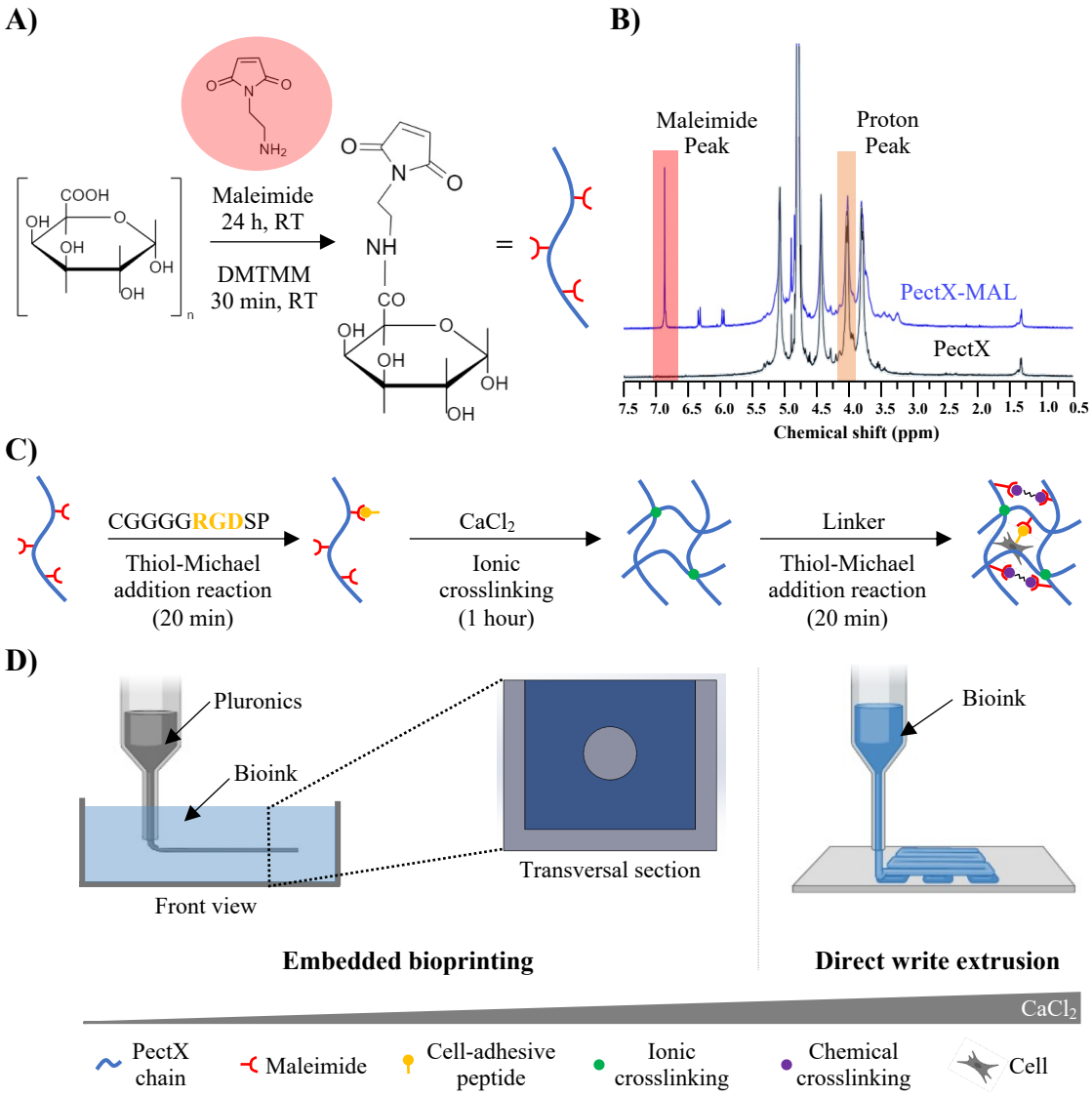

Figure 10: Schematic representation of hydrogel design, fabrication and 3D bioprinting. A) Chemical modification of pectin derivative (PectX) with maleimide functional groups by reaction with DMTMM. B) ^{1}H NMR spectra of PectX and PectX-MAL. C) Illustration of the design and preparation of the dual-crosslinked hydrogel bioink by combining ionic gelation and clickable Thiol-Michael addition reaction. D) Schematic illustration depicting the versatility of the PectX-MAL hydrogel for extrusion bioprinting via direct writing and embedded deposition strategies.

4.2. Rheological properties of the hydrogels

The first optimization of the experimental work was to determine the most suitable physical crosslinking degree to create hydrogels with proper rheology for processing via extrusion bioprinting. To do that, a systematic analysis on the impact of crosslinking degree on the injectability and filament formation was carried out by fixing the PectX-

MAL content at 2% and varying the $CaCl_2$ concentration in a range of 8-12 mM. By increasing the $CaCl_2$ concentration it was possible to observe an increase in the solution viscosity and the formation of a more stable filament. This can be explained by the presence of more divalent ions in solution for the same density of carboxyl groups, which increases the hydrogel crosslinking degree. However, the $CaCl_2$ concentration cannot be increased indefinitely due to the fact that for higher concentrations there will be an imbalance on the ratio of carboxylic groups to divalent ions, resulting in the formation of a heterogeneous hydrogel, which is characterized by an irregular filament and a two-phase sol-gel solution.

To determine the ionic gelation kinetics, crosslinked hydrogels were prepared with different final $CaCl_2$ concentrations (8-12, and the evolution on the elastic (G') and viscous (G'') modulus was determined by rheometry **(Figure 11A)**. Regardless of the $CaCl_2$ concentration, it was possible to observe a great oscillation on both G' and G'' in the first minutes after $CaCl_2$ addition, which tended to stabilize throughout time. In all the hydrogel formulations, the G' and G'' reached the plateau within 3600s, but their value showed a dependency on the $CaCl_2$ concentration. To better understand the influence of the $CaCl_2$ content on the mechanical properties of hydrogels, we calculated the average storage modulus on equilibrium by considering all time points with a variation of ±10% from the value reached at 3600s **(Figure 11B)**. As expected, the G' increased with higher $CalCl_2$ concentrations, which can be explained by an increase on the density of physical crosslinks in the hydrogels (0 mM $CalCl_2$: G' 25.55 ± 0.39 Pa; 8 mM $CalCl_2$: G' 176.10 ± 4.88 Pa; 10 mM $CalCl_2$: G' 417.40 ± 12.76 Pa; 12 mM $CalCl_2$: G' 1029.00 ± 30.31 Pa).

The shear-thinning behavior, which is the ability of a bioink to decrease its viscosity beyond a critical shear rate, is an important characteristic for a bioink to be extruded through the nozzle [70]. To evaluate this characteristic, shear viscosity tests **(Figure 11C)** were conducted, which confirm that all hydrogel formulations present the ability to flow with minimal resistance through the nozzle. It was possible to conclude that all $CaCl_2$ concentrations studied exhibited a shear-thinning behavior, characterized by a decrease in the viscosity as the shear rate increases, which is fundamental for the extrusion bioprinting process. Furthermore, it is also possible to observe that the highest $CaCl_2$ concentration (12 mM) resulted in the highest shear viscosity value which is

related to superior physical crosslinking of the gel network. As expected, reducing the $CaCl_2$ concentration (8-10 mM) led to a decrease in the shear viscosity of hydrogels.

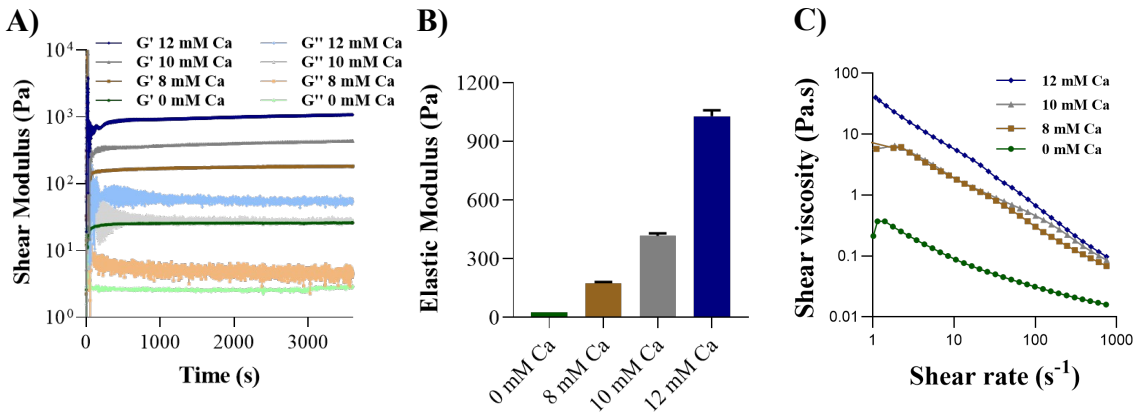

Figure 11: Rheological properties of hydrogels. A) Influence of the $CaCl_2$ concentration on the ionic gelation kinetics of hydrogels prepared at 2% polymer concentration. B) Elastic moduli of ionically crosslinked hydrogels at the equilibrium (values were determined considering a variation of ±10% from the value reached at 3600s). C) Viscosity profile of ionically crosslinked hydrogels prepared using different $CaCl_2$ concentrations.

4.3. Mechanical properties and cell response in 3D hydrogels

In order to evaluate the ability of the developed hydrogels in instructing cell response as it happens in native ECM, the tunning of hydrogel mechanical properties and its effect on the response of dermal fibroblasts were studied in detail. To modulate the hydrogel mechanical properties, the concentrations of polymer, $CaCl_2$ and crosslinker were independently varied and the mechanical properties were analyzed **(Figure 12A)**. Overall, the *G′* of the hydrogels increased as function of higher concentrations of polymer, $CaCl_2$ and crosslinker, indicating that all parameters can be explored to tune the stiffness of the gel network. By increasing the $CaCl_2$ concentration from 8 to 12 mM, it is possible to observe that the *G′* ranged from 3033.00 ± 384.40 to 3840.00 ± 568.70 Pa, which corresponds to a 1.27-fold increase. As this effect is a result of higher physical crosslinking density of hydrogels, it should be pointed out that both the rheology and printability of hydrogels is also affected when changing the $CaCl_2$ concentration. Similarly, enhancing the concentration of the non-degradable crosslinker (DTT) from 0.125 to 0.5 mM led to a significant increase in the *G′* of hydrogels (3515.00 ± 442.60 to 4989.00 ± 542.20 Pa, 1.42-fold increase). This is explained by the

availability of more thiol groups to react with the maleimide groups in the PectX-MAL, leading to enhanced chemical crosslinking. Moreover, by increasing the polymer content from 2 to 3% there was also an increase of the elastic modulus (from 3840.00 ± 568.70 to 5860.00 ± 386.10 Pa, 1.53-fold increase) due to the fact that there are more carboxylic and maleimide groups available for crosslinking.

The design of ECM-mimetic hydrogels needs to fulfill several requirements, being the degradation an important one. This is essential to allow not only the clearance of foreign materials from the body, but also the controlled hydrogel degradation for cell proliferation, migration and ECM remodeling [95]. In this regard, we selected crosslinkers with different susceptibility to degradation by the action of cell secreted MMPs and evaluated their impact on both hydrogel mechanical properties and cell spreading. In detail, DTT was used as a non-degradable crosslinker, while the peptide sequences CGPQG↓IWGQC and CVPMS↓MRGGC were selected due to their lower and higher susceptibility to degradation, respectively, by a wide range of MMPs (e.g. 1, 2, 3 and 9) present in native skin [95].

To compare the results, a crosslinker concentration of 0.125 mM was used for hydrogel formation, while keeping fixed the polymer (2%) and $CaCl_2$ (10 mM) content. Results indicate that hydrogels fabricated by using MMP-degradable peptides formed slightly softer hydrogels (MMP: 2593.00 ± 261.50 Pa; MMP+: 2763.00 ± 449.50 Pa) compared to gels crosslinked with DTT (3515.00 ± 442.60 Pa). The fact that the molecular weight of the crosslinkers (DTT: 154.25 g/mol; MMP: 1048.20 g/mol; MMP+: 1040.32 g/mol) are different can impact the mechanical properties of the hydrogels. Furthermore, these results can also be related to the fact that hydrogels were incubated in DMEM supplemented with FBS, which can lead to some enzymatic degradation of hydrogels and result in lower mechanical properties. In fact, similarly observations were reported in a previous work using either PEG-fibrinogen or fibrin hydrogels. Specifically, the storage modulus of acellular PEG-fibrinogen and fibrin hydrogels progressively deteriorated over the course of 7 days of incubation in FBS-containing medium [102]. In another study using a series of enzymatically degradable PEG hydrogels with tunable degradability, the authors also concluded that the degradation rate of hydrogels was positively correlated with the use of MMP-degradable crosslinkers and negatively correlated with non-degradable ones. Most

importantly, hydrogels crosslinked with the non-degradable crosslinker showed superior mechanical properties due to more entanglements in PEG hydrogels [103].

The complex structure and composition of native skin, along with the use of multiple tests to characterize the mechanical behavior results in a wide range of the reported mechanical properties for the skin [104]. Morgan *et al* [105] used shear rheology to analyze whole human skin biopsies and dermis-only biopsies, and verified that the elastic and viscous modulus increase with the frequency oscillation (0.1 to 12 Hz). The mean G' and G'' modulus in the whole skin samples increased over the frequency range from 325.00 ± 93.70 to 1227.90 ± 498.80 Pa and 68.50 ± 21.20 to 189.90 ± 56.00 Pa, respectively, while the dermis-only samples showed a similar tendency with G' and G'' values increasing from 434.90 ± 122.10 to 6620.00 ± 849.50 Pa and 126.30 ± 34.50 to 458.90 ± 134.90 Pa, respectively. This behavior was explained based on the higher rate of increase in G' and G'' at higher frequencies (>1.59 Hz) in the dermis-only in comparison to the whole skin. Moreover, they concluded that the viscoelastic components of the dermis dominate at higher frequencies due to the inability of the viscous components to adapt to the rate of load application. In a similar study, Soeur and colleagues [106] characterized the mechanical properties of both human skin samples and *in vitro* skin biomimetic models through an amplitude sweep assay at 1 Hz with strains increasing from 0.01% to 0.1%, using a rheometer. The *in vitro* models were developed to recreate either the dermal layer only or full-thickness skin. To do that, fibroblasts were mixed with porcine acellular dermal matrix (2×10^6 cells/mL) and bovine type I collagen (1×10^6 cells in 7 mL collagen) were mixed with fibroblasts and bioprinted to create two distinct dermal models. After 4 days in culture, selected models were seeded with keratinocytes to reconstruct the epidermis layer. Results showed that full-thickness native human skin samples presented an elastic modulus ranging from 1800.00 to 5900.00 Pa. Moreover, the full-thickness model using dECM from porcine showed an elastic modulus (1800.00 to 7100.00 Pa) closer to that of native skin in comparison to the dermis layer only (900.00 Pa to 3000.00 Pa). The dermal-collagen and full-thickness collagen models exhibited much lower elastic modulus with values ranging from 900 Pa to 1200.00 Pa and 1000.00 to 3100.00 Pa, respectively. Based on these data, it is possible to conclude that the presence of an epidermal layer improved the mechanical properties of *in vitro* skin models. Overall, the strategy implemented in this work allows to develop dual-crosslinked hydrogels with

tunable elastic modulus ranging from 2593.00 to 5860.00 Pa, which are in the range of the elastic modulus of native human skin (≈1000.00-6000.00 Pa).

After characterizing the mechanical properties of hydrogels, the influence of hNDFs density within hydrogels (2.5×10^6 cells/mL, 5×10^6 cells/mL, 10×10^6 cells/mL, 20×10^6 cells/mL) was studied by analyzing the cell metabolic activity **(Figure 12B)** and fibronectin deposition **(Figure 12C)** after 14 days of culture in hydrogels containing 0.125 mM of the MMP+ crosslinker (2% PectX-MAL, 2 mM RGD, 10 mM $CaCl_2$). The MMP+ peptide crosslinker was selected to create the hydrogels as it is reported to allow enhanced MMP-mediated degradation and, therefore, facilitate cell spreading, proliferation and ECM deposition. Results indicated that with increasing cellular density within hydrogels it is possible to observe that the metabolic activity tends to remain more constant, with lower variations throughout the 14 days of culture. This can be explained due to the fact that lower cellular density allows the cells to have more space to spread and proliferate, while higher densities form more crowded gels. Confocal microscopy imaging of the gels shows that a cell density of 10×10^6 cells/mL creates a more homogenous cellular network with uniform deposition of fibronectin throughout the gel. Otherwise, lower cellular concentrations (2.5×10^6 cells/mL and 5×10^6 cells/mL) evidence almost no fibronectin deposition, which can be attributed to the fact that cells are sparsely populated in the gel network. Lastly, the highest cellular density (20×10^6 cells/mL) led to the deposition of a heterogeneous fibronectin network, which can be related with the excess of cells in the hydrogel and their reduced metabolic activity as depicted in **Figure 12B**. Based on these data, a cell density of 10×10^6 cells/mL was selected for subsequent studies.

The next step was to evaluate the influence of the matrix stiffness on the response of dermal fibroblasts. For that, hNDFs were mixed in different polymer formulations and its behavior was evaluated after 7 days of culture **(Figure 12D)**. Results showed that increasing the stiffness of the DTT-crosslinked hydrogels (2% PectX-MAL, 2 mM RGD, 0.125 mM DTT) through the addition of higher $CaCl_2$ concentrations results in enhanced cell spreading in 3D. Moreover, regardless the $CaCl_2$ concentration, it was possible to observe a uniform cell distribution at the center and periphery of the hydrogel, though cells exhibited a typical spindle-shaped morphology and established more cell-cell interactions in hydrogels containing higher $CaCl_2$ concentration. These data indicate that higher $CaCl_2$ concentrations (10-12 mM) provide a more favorable

environment to cells promoting their extensive spreading. Therefore, increasing the density of physical crosslinks in the gel and, consequently, increasing the elastic modulus (3033.00 to 3840.00 Pa) does not inhibit the capacity of the cells to locally remodel the hydrogel network. Notably, as these gels are not susceptible to cell-mediated network degradation, we hypothesize that cells are able to locally remodel the gel network for cell spreading despite the relatively higher G' values.

When comparing the impact of DTT concentration (2% PectX-MAL, 2 mM RGD, 10 mM $CaCl_2$), it is possible to observe that increasing the DTT concentration from 0.125 to 0.50 mM, the cells presented a rounder shape, despite the uniform distribution in the gel. This result indicates that a higher crosslinked network creates a more restrictive environment, hindering the ability of the cells to remodel the surrounding niche.

Regarding the effect of the crosslinker, it was found that cells exhibited a higher spreading ability and showed a spindle-shape morphology when embedded within hydrogels (2% PectX-MAL, 2 mM RGD, 10 mM $CaCl_2$) crosslinked with the MMP-sensitive peptide crosslinker (CGPQG↓IWGQ) compared to those crosslinked using the non-degradable crosslinker (DTT). Despite the concentration of both crosslinkers was fixed (0.125 mM), the results suggest that cells were able to degrade the MMP-sensitive peptide in order to remodel the gel network and acquire a spread morphology. Cell-laden hydrogels were cultured in the presence of a broad-spectrum of MMP inhibitor (Marimastat) to assess whether cell spreading was exclusively dependent on MMP-mediated hydrogel degradation. Results showed that for hydrogels with low crosslinking density ($G' = 70.03 \pm 10.39$ Pa) the matrix stiffness was a key parameter influencing cell spreading, while in stiffer hydrogels ($G' > 143.09 \pm 29.70$ Pa) the major driver for cell elongation was the ability of the cells to degrade the MMP-cleavable crosslinker. Overall, these data indicate that the presence of the MMP-degradable peptide sequence influences cell spreading [107]. Despite our findings being supported by literature, further characterization regarding the secretion of MMPs or their inhibition using a MMP inhibitor would be useful to assess whether cell spreading and morphology are exclusively dependent of the MMP peptide and not related with the stiffness of the gel, which is slightly lower when compared to the DTT-crosslinked hydrogel.

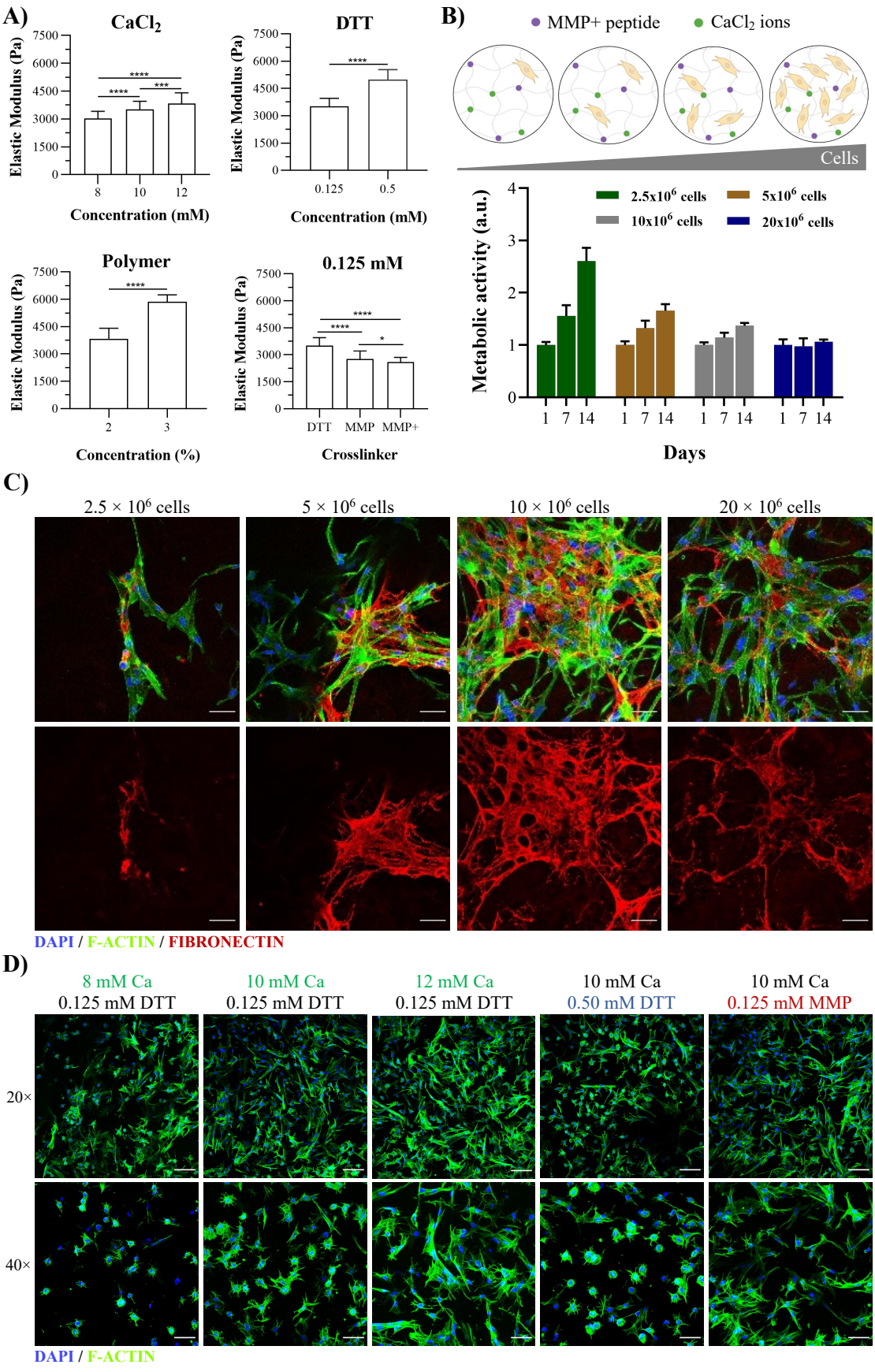

Figure 12: Mechanical tunability of hydrogels and the impact of mechanical cues on the response of dermal fibroblasts in 3D. A) Influence of $CaCl_2$, chemical crosslinkers and polymer

concentration on the elastic modulus of dual crosslinked hydrogels. B) Effect cell density on the metabolic activity of cell-laden hydrogels at day 1, 7 and 14 of culture. C) Confocal images depicting the cell morphology and ECM deposition within hydrogels (2 % PectX-MAL, 2 mM RGD, 10 mM $CaCl_2$) crosslinked with the MMP+ peptide (CVPMS↓MRGGC, 0.125 mM) and cultured with different densities of dermal fibroblasts stained for nuclei (blue), F-actin (green) and fibronectin (red) at day 14 (scale bar: 50 µm). D) Representative confocal images of dermal fibroblasts stained for nuclei (blue) and F-actin (green) showing the effect of hydrogel (2 % PectX-MAL, 2 mM RGD) stiffness, modulated via ionic and chemical crosslinking (MMP: CGPQG↓IWGQC), on cell morphology within gels at day 7 of culture (scale bars: 100 µm (20x); 50 µm (40x); *$P < 0.05$; ***$P < 0.001$; ****$P < 0.0001$)

4.4. Effect of biochemical and biophysical cues on ECM deposition within 3D hydrogels

A major function of fibroblasts in the skin is the synthesis and remodeling of ECM, which is essential for maintaining the functional properties of the skin and assure tissue homeostasis. Based on the experimental data regarding the effect of hydrogel properties on cell morphology and spreading, we selected the best-performing hydrogel formulation (2% Pect-MAL, 2 mM RGD, 10 mM $CaCl_2$ and 10×10^6 cells/mL) to evaluate the impact of the chemical crosslinker on the ability of hydrogels to support *de novo* ECM deposition. To do that, different types of crosslinkers, namely DTT, MMP and MMP+ peptides, were used to chemically crosslink cell-laden hydrogels. After 7 and 14 days of culture, hydrogels were fixed and stained for fibronectin **(Figure 13A)**. At day 1, cells embedded within hydrogels crosslinked with MMP-degradable peptides displayed a more homogenous cell distribution and exhibited a typical spindle-shape morphology in comparison to DTT-crosslinked hydrogels. At day 7, despite all hydrogel formulations supporting the deposition of an interconnected fibronectin network, confocal microscope imaging suggests the presence of a denser and more homogeneous fibronectin network in hydrogels crosslinked with MMP-degradable peptides. At a later time period (day 14), similar results were observed, indicating that the introduction of MMP-sensitive peptides in the gel network favor the deposition of a more uniform protein network in 3D hydrogels. However, additional characterization to quantify the protein levels in each hydrogel is warranted to support the data from confocal microscopy. Collectively, these data indicate that, for long term cell culture, the use of the MMP+ peptide promotes the *de novo* ECM deposition of larger amounts

of fibronectin. This can be explained by the ability of fibroblasts to degrade the peptide crosslinker and, therefore, create space to spread and remodel the surrounding environment towards ECM deposition. However, it is also important to highlight that despite differences in the amount of fibronectin deposition, all hydrogels supported its deposition regardless the type of crosslinker used for hydrogel formation. In addition to the altered hydrogel biochemical cues derived from the crosslinker, the cell behavior can also be affected by the different mechanical properties of the hydrogels. In fact, there is a coupling between the biochemical and biophysical cues as changing the crosslinker type leads to altered mechanical properties of hydrogels. The metabolic activity of the hydrogels was also evaluated after 1, 7 and 14 days of culture **(Figure 13B)**. The data shows that the hydrogel crosslinked with the MMP+ peptide has constant metabolic activity, with a slight decrease after 14 days of culture. In addition, the hydrogel crosslinked with the MMP peptide shows a decrease at day 7, but it remains constant after 14 days of the assay, while DTT-crosslinked hydrogels displayed a little decrease in all time points. Accordingly, it is possible to conclude that the tested hydrogels formulations do not influence the metabolic activity of the cells, which indicates that all chemical crosslinkers create hydrogels with favorable conditions to maintain metabolically active cells in 3D. However, DNA quantification and counting the cell number in hydrogels would provide additional data to further characterize how hydrogel properties impact cell response.

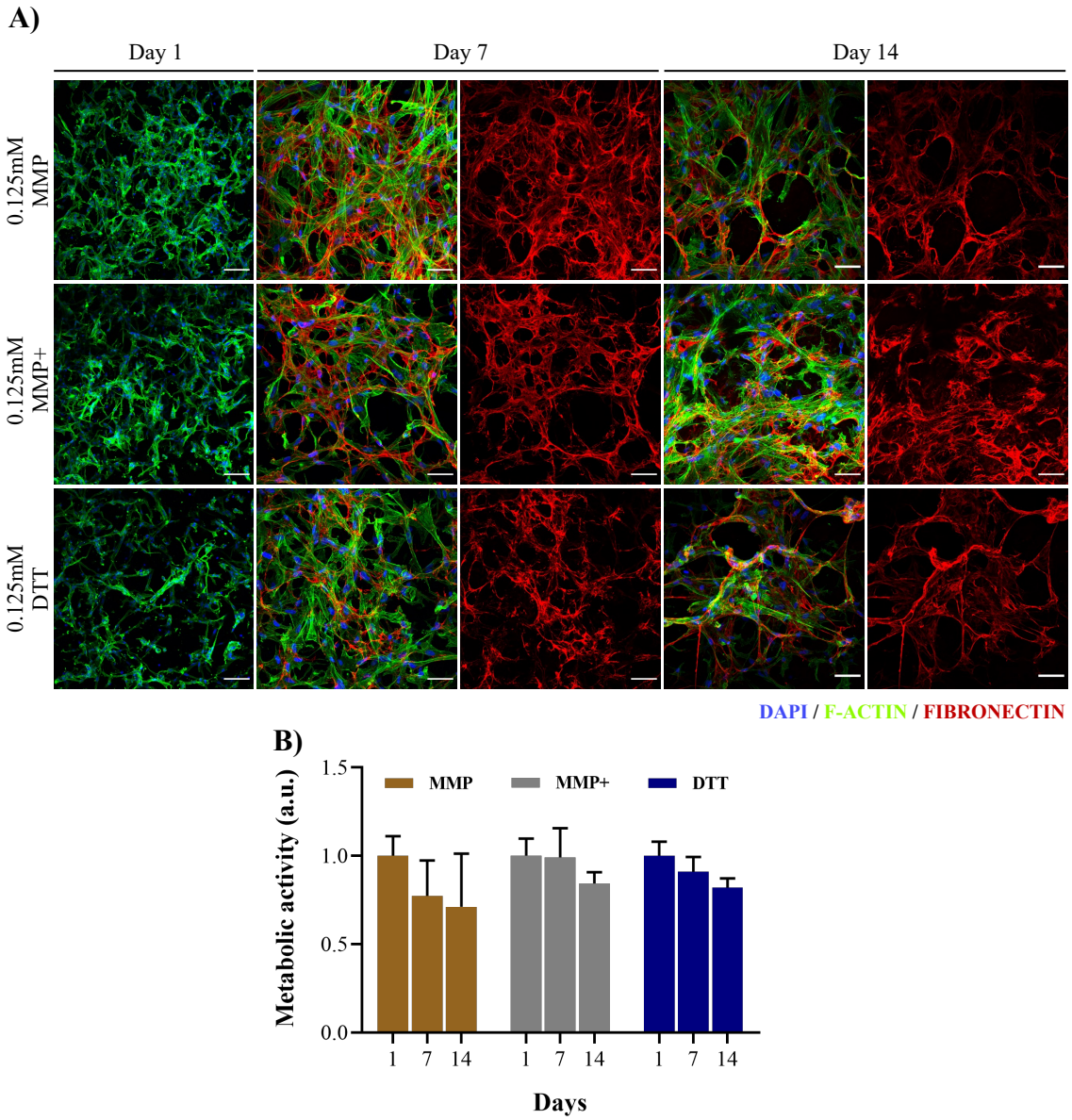

Figure 13: Influence of hydrogel properties on *de novo* ECM deposition. A) Representative confocal microscopy images showing the influence of the chemical crosslinker (MMP: CGPQG↓IWGQC; MMP+: CVPMS↓MRGGC; and DTT) on the morphology of dermal fibroblasts and fibronectin deposition within 3D hydrogels at day 1, 7 and 14 of culture (nuclei: blue, F-actin: green, and fibronectin: red; scale bars: 100 µm (day 1), and 50 µm (days 7 and 14)). B) Metabolic activity of cell-laden hydrogels at day 1, 7 and 14.

4.5. Establishment of bioengineered 3D models of skin burn wounds

Burn injuries are one of the leading causes of skin injury worldwide often causing physical scarring, extensive pain, morbidity and mental issues to the patient. Nowadays, the gold-standard to treat burn injuries relies on the use of skin grafts or skin substitutes depending on the severity (depth and extension) of the lesion. Although some

improvements have been made throughout the years regarding patient survival following severe burn injury, new therapeutic approaches to improve burn outcomes (e.g., scarring) are urgently needed [26]. In order to reach this milestone, it is fundamental to understand the physiological mechanisms triggered after a burn episode, as well as how different burn wounds lead to distinct cell responses (e.g., activation, apoptosis, necrosis) and ECM remodeling. To address this unmet need, in this work skin biomimetic models resembling either dermis-only or bilayered skin (dermis and epidermis layers) were established and employed to create 3D burn wound models by inducing a thermal burn injury in healthy models. Such models were subsequently used to evaluate the impact of the burn injury in cell viability.

The first experiments were performed on the 3D models of the dermis, following the schematic workflow shown in the **Figure 14A**. Specifically, the model was kept in culture for 28 days to match the culture time of bilayer skin models, followed by the application of a contact burn injury using a stainless-steel rod at 65 ºC for 120 seconds on the center of the model **(Figure 14B)**. In order to study the efficacy of this approach in creating a burn wound, a first proof-of-concept was carried out using small volume hydrogels (20 µL) cultured for 7 days. After 24 hours of injury, samples were imaged for live/dead analysis, which showed that cells were dead in the hydrogel subjected to burn injury, while the majority of the cells were alive in the control hydrogel (without burn injury) **(Figure 14C)**. Therefore, it was possible to conclude that the developed approach allows to induce a burn wound characterized by a dramatic decrease in cell viability. Based on these data, the same methodology was applied to create a larger and thicker dermal burn model (300 µL hydrogel, 28 days of culture). When compared to the control model, a contact burn was clearly visible as a circle area in the center of the dermis-only model **(Figure 14D)**. After 1 day of injury, cell viability was analyzed through live/dead assay to evaluate whether the impact of burn injury is limited to the contact region with the heated bar **(Figure 14E)**. Results showed that no dead cells were stained in the burn sample, while the majority of the cells were alive with a homogeneous distribution. Furthermore, after 7 days of injury, cell viability was analyzed through live/dead assay and the results indicated a significant increase in the number of dead cells on the region of the burn injury in comparison to the periphery of the model **(Figure 14E)**. Furthermore, the control sample clearly showed that most of the cells were alive and presented a homogeneous distribution and characteristic

spindle-shaped morphology throughout the model. As the live/dead assay uses propidium iodide as a marker of necrotic cells, we hypothesise that the lack of staining at day 1 after injury can be due to the fact that cells are under programmed cell death (apoptosis) instead of unprogrammed cell death due to cell injury (necrosis). However, further studies are required to confirm this hypothesis and distinguish apoptosis from necrosis, which can be done by staining the cells using Annexin V (apoptosis marker). The models were also characterized by histology at day 1 post-injury using H&E and Masson's Trichrome staining **(Figure 14F)**. Results showed the homogenous distribution of fibroblast cells throughout the model as well as the deposition of collagen, though no significant differences between the control and the burn model are observed. This can be related to the fact that the histological analysis was done after 1 day of burn injury and with the experimental approach implemented to create the burn wound. Therefore, further optimization of the temperature of the stainless-steel rod and the contact time are necessary as well as the histological analysis being done a few days later after the creation of the burn wound.

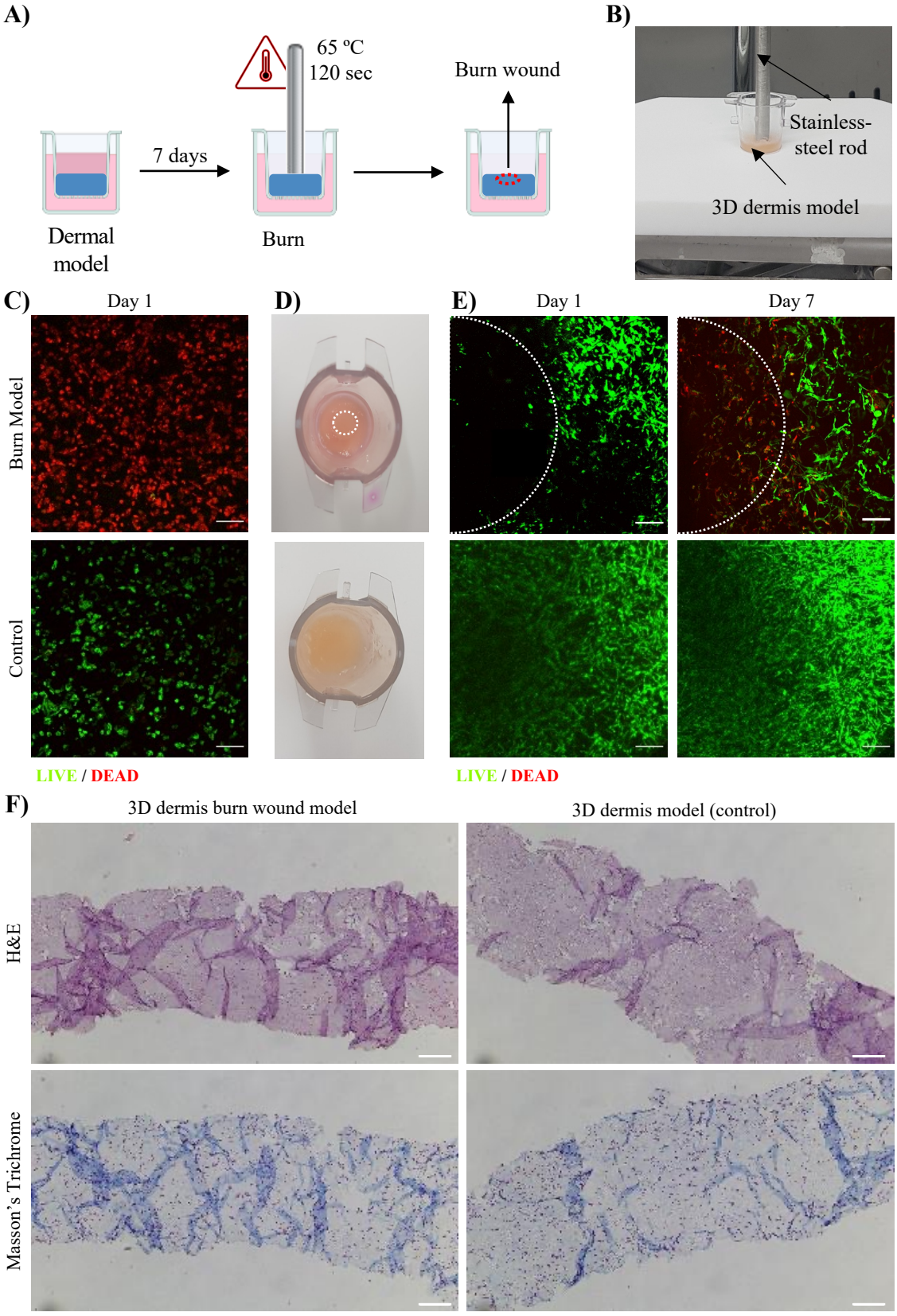

Figure 14: Establishment and characterization of the *in vitro* 3D dermal burn wound model. A) Schematic illustration of experimental approach to create the burn wound using a 3D model of the dermis. B) Experimental setup implemented to create the burn wound using a heated

stainless-steel rod in contact with the surface of the model (65ºC, 120 s). C) Representative confocal microscopy images of Live/Dead staining of fibroblasts-laden hydrogels after 1 day of burn injury (scale bar: 100 μm). D) Photographs of the *in vitro* skin models either with or without the burn injury. E) Representative confocal microscopy images of Live/Dead staining of the *in vitro* dermis skin model after 1 and 7 days of burn injury (dash line indicates the interface between the healthy and burn regions); scale bar: 100 μm. F) H&E and Masson trichrome staining's of the *in vitro* dermis burn wound models either with or without the burn injury (scale bar: 200 μm).

Native skin comprises multiple cells such as fibroblast, keratinocytes, immune cells and endothelial cells, which are essential to impart skin properties and functions, as well as for wound healing [108]. Therefore, the second approach aimed at creating a bilayer skin model consisting of both fibroblasts and keratinocytes as the cellular components to resemble the dermis and epidermis layers, respectively **(Figure 15A)**. Briefly, after 7 days of culture to create the dermis, HaCaT cells were seeded on top of the dermal layer and cultured submerged for 7 days to allow cell attachment and proliferation. Next, the bilayer model was raised to the ALI for 14 days to promote the formation of a stratified and differentiated epidermis. Finally, the same experimental approach as described before was followed to create the burn injury. In order to determine the impact of cell seeding density on epidermis formation, HaCaT cells were seeded at different densities ($1x10^6$ cells, $1.5x10^6$ cells, $2x10^6$ cells, $2.5x10^6$ cells) onto the dermis **(Figure 15B)**. Results show that the lower cell densities do not allow to create a homogenous epidermal layer as shown by the appearance of some irregular regions on the model. On the other hand, on the highest cell density it is visible that the epidermal layer starts to be pulled out in some regions, which can be explained by the excess number of cells that are being used. Accordingly, $2x10^6$ cells seemed to be the most suited cell density to form a regular cellular distribution and a homogenous epidermal layer. To assess the effect of the burn injury on the model, live/dead analysis was performed at day 1 post-injury **(Figure 15C)**. Results clearly show the presence of an interface between the burn region and the intact model marked by a dramatic difference in the number of live cells. Notably, live cells were only detected in the non-burn region, while neither live nor dead cells were observed in the burn region. As mentioned before, for the dermis-only model, these results can be explained by a state of cellular apoptosis at day 1 of injury, while there is a necrosis state at day 7 of injury. Therefore, further studies are required to support our hypothesis and characterize the cell response. Moreover, the epidermal

layer can also provide protection to the dermal layer from the thermal injury, which can also impact the cell response as reported in other works [106].

Histologically, staining for H&E and Masson's Trichrome after 1 day of injury showed that the *in vitro* control model supported the formation of a full-thickness skin, with morphological resemblance to the human skin **(Figure 15D)**. H&E staining of the control model showed that the dermal compartment is uniformly populated with dermal fibroblasts, while keratinocytes formed a well-defined epidermis layer on top of the fibroblast-laden hydrogel after 14 days of ALI culture. The Masson's Trichrome staining revealed that fibroblasts were secreting collagen, a major component of the skin ECM as observed by a homogeneous blue staining in the dermal layer. Although immortalized keratinocytes have been successfully used to reconstruct the epidermal layer in 3D skin models, the use of these cells presents some limitations as they evidence loss of cell phenotype and function which can lead to abnormal epidermal stratification [109]. Histological analysis of the 3D burn wound model reveals a disruption of the epidermal and dermal layers, which can be attributed to the burn injury induced by the model as this is absent in the control models. However, it should be pointed out that this disruption could also be a combined effect of the altered and probably more fragile properties of the model due to the injury and potential artifacts related to the processing of the models for histological analysis. Thus, further analysis is required to better characterize the skin models and the impact of burn injury to the models. For example, immunohistological analysis of specific markers for epidermal differentiation and proliferation (e.g., cytokeratin, Ki67), as well as for the dermal layer (e.g., vimentin, Coll-I, fibronectin) would provide more meaningful and comprehensive data.

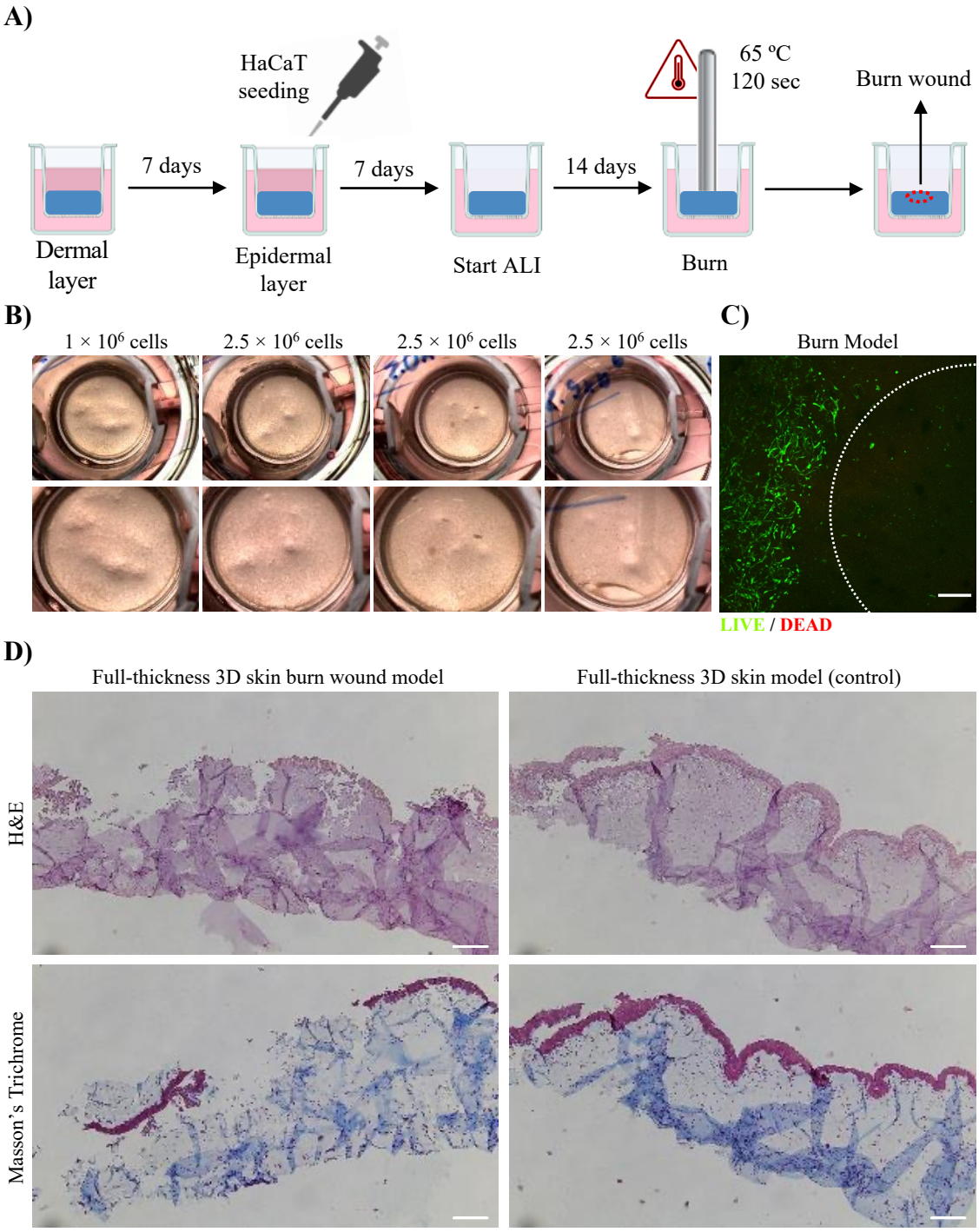

Figure 15: Establishment and characterization of the *in vitro* full-thickness 3D skin burn wound model. A) Schematic illustration of experimental approach to create the bilayer skin burn wound model. B) Photographs of the *in vitro* bilayer models created using different densities of keratinocytes. C) Representative confocal microscopy image of Live/Dead staining of the *in vitro* bilayer model after 1 day of burn injury (dash line indicates the interface between the healthy and burn regions) (scale bar: 100 µm). D) H&E and Masson trichrome staining's of the *in vitro* bilayer skin models either with or without the burn injury (scale bar: 200 µm).

4.6. Proof-of-concept demonstration of the establishment of skin burn wound model on-a-chip

As animal models present limitations in accurately predict the performance of new drugs and therapies in human clinical trials, it is crucial to develop more reliable and biomimetic skin models that can truly recapitulate key (patho)physiological aspects of healthy and diseased skin to be used as viable alternatives to animal testing [110].

Skin-on-a-chip models are emerging as one of the most promising approaches to develop advanced and more reliable models as the possibility to connect with microfluidic pumps allows the perfusion of culture media to provide nutrition to the models or even the perfusion of cells to better recapitulate key features of human tissues and organs (e.g., vascular system). In fact, the ability to engineer 3D vascularized constructs that mimic natural tissues requires several key components, including cells, ECM and vascularization, which impart, support and sustain the biomimetic function of the engineered tissue construct. However, current tissue engineered constructs still lack to complete resemble all these key components. In fact, recreate the vascular network has been reported to be not only one of the most critical challenges, but also one of the most important ones as the absence of functional vascularization led to deficient nutrition supply, cell-cell and cell-ECM interactions and, consequently, quickly development of necrotic regions [111, 112]. To surpass this limitation, 3D printing technology emerged as a promising solution by creating customized sacrificial channels which can be removed after the printing process, leaving hollow channels that enable perfusion of nutrients or even the seeding of endothelial cells to form a blood vessel network [113].

In this work, a proof-of-concept of a skin-on-a-chip was created following the schematic workflow shown in the **Figure 16A**. Briefly, a Pluronic F127 biomaterial ink was 3D printed onto a glass slide to serve as an outer mold, which in a later stage would be made of PDMS to confer mechanical resistance. Then, an ionically crosslinked hydrogel (2% Pect-MAL, 2 mM RGD, 8 mM $CaCl_2$ and 10×10^6 cells/mL) loaded with fibroblasts was manually casted onto the mold, followed by the embedded printing of the Pluronic F127 biomaterial ink to create a perfusable channel. Afterwards, a solution of DTT (0.125 mM) was pipetted onto the hydrogel for chemical crosslinking. Finally, by exploring the thermosensitive properties of Pluronic F127, the construct was placed

on ice to liquify the Pluronic F127 and remove the sacrificial channel, leaving hollow channel inside of the hydrogel. To demonstrate the efficiency of the approach, fluorescein was perfused through the channel to better visualize the hollow channel in 3D.

Despite in this proof-of-concept experiment the hydrogel was manually casted onto the Pluronic F127 mold, we have also bioprinted the cell-laden hydrogel to assess the impact of the extrusion process on cellular viability. Live/Dead analysis showed that the majority of the cells were alive at day 1 post-printing with almost no dead cells visible **(Figure 16B)**. Furthermore, after 7 days of culture, the cells exhibited a homogeneous distribution with typical spindle-shaped morphology and established cell-cell interactions **(Figure 16B)**. Overall, this data indicates that the bioprinting process does not affect cell viability, morphology and spreading.

A major functional requirement of a 3D skin-on-a-chip is the presence of a perfusable channel and/or functional vasculature, which allow the transport and supply of nutrients to cells in order to avoid the formation of a necrotic tissue. Therefore, to assess if the adopted embedded bioprinting strategy could induce damage to cells within the hydrogel, Live/Dead assay was performed after 1 day of printing **(Figure 16C)**. Results clearly evidence that almost all the cells were alive with no visible dead cells. Furthermore, it is also visible that the hollow channel maintained the structural integrity within the hydrogel, showing the ability of the printing strategy to generate hollow channels in 3D. Finally, after 7 days of culture, confocal microscope images indicate that cells acquired a characteristic spindle-shape morphology **(Figure 16C)**. Most importantly, the channel was still maintained in 3D despite the slight deformation in comparison to day 1, which can be related to the fact that the model was kept in culture without any perfusion throughout the experiment.

In summary, an embedded bioprinting strategy was applied to develop a perfusable hydrogels in a customized 3D printed chip. This approach opens new avenues towards the development of an *in vitro* 3D burn skin-on-a-chip that better resembles the native environment. Finally, with some optimizations such as the integration with microfluidics technology, this approach could allow us to develop an *in vitro* burn skin biomimetic model with integrated vascularization to better understand the biological mechanisms and wound healing process underlying the burn injury, as well as to allow development and screening of new therapies to treat burn injuries.

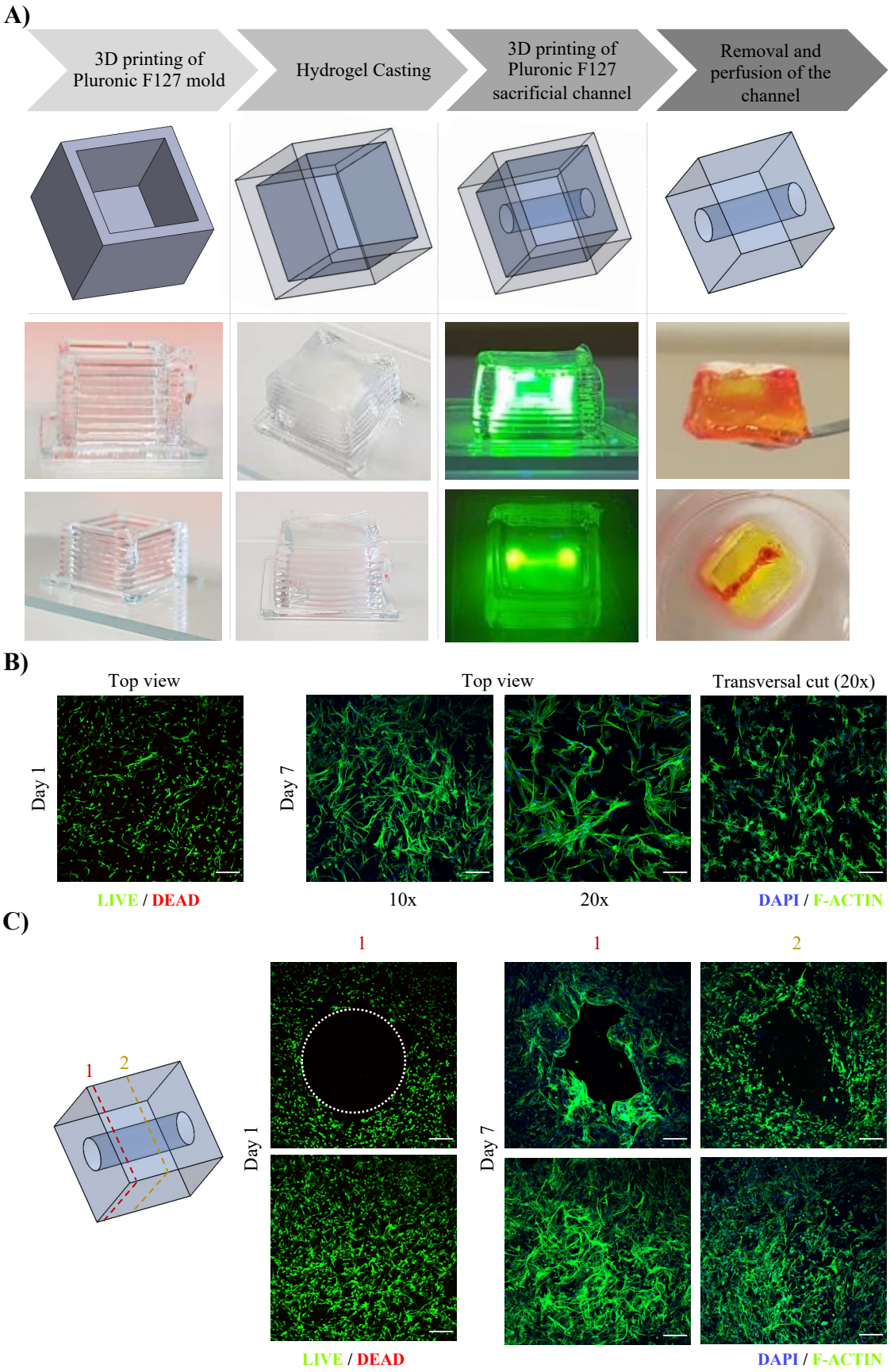

Figure 16: Establishment of the skin model on-a-chip. A) Schematic illustration of the experimental approach to create the perfusable hydrogel construct using a sacrificial

material in a customized 3D printed chip and the experimental results obtained. B) Representative confocal microscopy images of Live/Dead staining of the bioprinted hydrogel after 1 day of culture (scale bars: 200 μm) and staining for nuclei (blue) and F-actin (green) after 7 days (scale bars: 200 μm (10x); 100 μm (20x)). C) Representative confocal microscopy images of Live/Dead staining of the perfusable hydrogel after 1 day and staining for nuclei (blue) and F-actin (green) after 7 days (scale bars: 200 μm).

CHAPTER 5 – CONCLUSIONS AND FUTURE PERSPECTIVE

5. Conclusions and Future Perspectives

In this study, a bioprinting strategy was developed with the ultimate goal of fabricating pathophysiological relevant models of skin burn wounds.

The first step was to design a novel clickable bioink mimicking key features of native skin and allowing the processing through extrusion bioprinting following both traditional (i.e, direct writing) and advanced (i.e., embedded printing) fabrication strategies. The developed bioink, consisting of a pectin derivate functionalized with maleimide groups, thiolated chemical crosslinkers and cell-adhesive peptide ligands, allowed to implement a dual-crosslinking strategy with tunable rheological and mechanical properties. The bioink rheological properties were precisely adjusted via ionic gelation using calcium chloride, while the selection of the chemical crosslinker allowed us to modulate both hydrogel degradability and stability using a thiol-Michael addition click reaction. The bioink showed similar mechanical properties to the native skin and supported metabolically active cells throughout 14 days of culture. Furthermore, bioinks supported extensive spreading of dermal fibroblasts as well as deposition of fibronectin in 3D, though it was found that these parameters depend on both matrix stiffness and type of the chemical crosslinker used for hydrogel formation.

Biomimetic skin models were then developed by seeding keratinocytes seeded onto fibroblast-laden hydrogels. Results showed that the developed hydrogels supported the *in vitro* formation of full-thickness skin resembling the architecture and morphology of the native human skin. A burn injury created on the *in vitro* models using a stainless-steel rod induced a significant reduction in cellular viability on the wound area at 1 and 7 days post-injury. Overall, the developed experimental approach allowed us to create an *in vitro* skin model that recapitulates key hallmarks of skin burn wounds, namely the decrease of the cellular viability and disruption of the skin structure.

Lastly, 3D bioprinting allowed to engineer a perfusable hydrogel construct using a sacrificial material in a customized 3D printed chip. Indeed, the developed bioink supported the deposition of a sacrificial material following by embedded extrusion bioprinting. Cells remained alive 1 and 7 days after the extrusion process and, most importantly, the channel was kept open for 7 days without any perfusion throughout the experiment.

Overall, a bioengineered strategy was developed to create the first *in vitro* skin burn model with promising results and potential to be used for several tissue engineering applications, including disease modelling, drug screening and wound healing.

Future Perspectives

In order to improve the work developed in this dissertation, future works should be focused on the detailed analysis of burn injury and translation of the data towards the fabrication of a perfusable skin burn model on-a-chip.

First, evaluating the swelling and enzymatic degradation behavior of hydrogels would be important to understand the stability of the gels throughout the culture time. Furthermore, additional optimizations regarding the development of the burn wound such as culture time of the skin models, the diameter and temperature of the tool, as well as the duration of the contact between the tool and the *in vitro* model would be very important to optimize the wound extension and standardize the experimental protocol. In addition, a more detailed study using the *in vitro* skin burn model should be focused on testing the ability of well-known therapeutics (e.g., creams, growth factors) to improve the healing process upon injury. This would allow us to evaluate the healing ability of the developed model, which is important for its validation. Finally, a more sophisticated, perfusable and vascularized skin burn wound model-on-a-chip could be created via integration with microfluidics and additional cell types (e.g., endothelial cells, immune cells). Such a model would better reproduce the native environment and allow us to draw more biologically relevant conclusions regarding cellular effects of the burn wound.

References

[1] R.F. Pereira, C.C. Barrias, P.L. Granja, P.J. Bartolo, Advanced biofabrication strategies for skin regeneration and repair, Nanomedicine 8(4) (2013) 603-621.
[2] M. Takeo, W. Lee, M. Ito, Wound healing and skin regeneration, Cold Spring Harb Perspect Med 5(1) (2015) a023267.
[3] R.A.F. Clark, K. Ghosh, M.G. Tonnesen, Tissue Engineering for Cutaneous Wounds, Journal of Investigative Dermatology 127(5) (2007) 1018-1029.
[4] L. Yildirimer, N.T.K. Thanh, A.M. Seifalian, Skin regeneration scaffolds: a multimodal bottom-up approach, Trends in Biotechnology 30(12) (2012) 638-648.
[5] Human Wound and Its Burden: Updated 2020 Compendium of Estimates, Advances in Wound Care 10(5) (2021) 281-292.
[6] C. Lindholm, R. Searle, Wound management for the 21st century: combining effectiveness and efficiency, International Wound Journal 13(S2) (2016) 5-15.
[7] S.A. Eming, P. Martin, M. Tomic-Canic, Wound repair and regeneration: Mechanisms, signaling, and translation, Science Translational Medicine 6(265) (2014) 265sr6-265sr6.
[8] R.F. Pereira, A. Sousa, C.C. Barrias, A. Bayat, P.L. Granja, P.J. Bártolo, Advances in bioprinted cell-laden hydrogels for skin tissue engineering, Biomanufacturing Reviews 2(1) (2017) 1.
[9] A. Piaggesi, S. Låuchli, F. Bassetto, T. Biedermann, A. Marques, B. Najafi, I. Palla, C. Scarpa, D. Seimetz, I. Triulzi, P. Turchetti, A. Vaggelas, Advanced therapies in wound management: cell and tissue based therapies, physical and bio-physical therapies smart and IT based technologies, Journal of Wound Care 27(Sup6a) (2018) S1-S137.
[10] E. Sutterby, P. Thurgood, S. Baratchi, K. Khoshmanesh, E. Pirogova, Microfluidic Skin-on-a-Chip Models: Toward Biomimetic Artificial Skin, Small 16(39) (2020) 2002515.
[11] C.-M. Moysidou, C. Barberio, R.M. Owens, Advances in Engineering Human Tissue Models, Frontiers in Bioengineering and Biotechnology 8 (2021).
[12] Extracellular Matrix Reorganization During Wound Healing and Its Impact on Abnormal Scarring, Advances in Wound Care 4(3) (2015) 119-136.
[13] E. García-Gareta, Introduction to biomaterials for skin repair and regeneration, in: E. García-Gareta (Ed.), Biomaterials for Skin Repair and Regeneration, Woodhead Publishing2019, pp. xiii-xxvii.
[14] J.E. Lai-Cheong, J.A. McGrath, Structure and function of skin, hair and nails, Medicine 49(6) (2021) 337-342.
[15] C.A. Brohem, L.B. da Silva Cardeal, M. Tiago, M.S. Soengas, S.B. de Moraes Barros, S.S. Maria-Engler, Artificial skin in perspective: concepts and applications, Pigment Cell & Melanoma Research 24(1) (2011) 35-50.
[16] P.A.J. Kolarsick, M.A. Kolarsick, C. Goodwin, Anatomy and Physiology of the Skin, Journal of the Dermatology Nurses' Association 3(4) (2011) 203-213.
[17] J.M. Abdo, N.A. Sopko, S.M. Milner, The applied anatomy of human skin: A model for regeneration, Wound Medicine 28 (2020) 100179.
[18] A.D. Metcalfe, M.W. Ferguson, Tissue engineering of replacement skin: the crossroads of biomaterials, wound healing, embryonic development, stem cells and regeneration, J R Soc Interface 4(14) (2007) 413-37.
[19] J.S. Boateng, K.H. Matthews, H.N.E. Stevens, G.M. Eccleston, Wound Healing Dressings and Drug Delivery Systems: A Review, Journal of Pharmaceutical Sciences 97(8) (2008) 2892-2923.

[20] S. Guo, L.A. Dipietro, Factors affecting wound healing, J Dent Res 89(3) (2010) 219-29.
[21] J.M. Reinke, H. Sorg, Wound Repair and Regeneration, European Surgical Research 49(1) (2012) 35-43.
[22] A.C. Gonzalez, T.F. Costa, Z.A. Andrade, A.R. Medrado, Wound healing - A literature review, An Bras Dermatol 91(5) (2016) 614-620.
[23] M. Xue, C.J. Jackson, Extracellular Matrix Reorganization During Wound Healing and Its Impact on Abnormal Scarring, Adv Wound Care (New Rochelle) 4(3) (2015) 119-136.
[24] A.B. Association, "Burn Incidence Fact Sheet", *Burn Incidence and treatment in the United States: 2016*, 2016. https://ameriburn.org/who-we-are/media/burn-incidence-fact-sheet/. (Accessed 17 August 2022).
[25] WHO, Burns, 2018. https://www.who.int/news-room/fact-sheets/detail/burns. (Accessed 17 August 2022).
[26] M.G. Jeschke, M.E. van Baar, M.A. Choudhry, K.K. Chung, N.S. Gibran, S. Logsetty, Burn injury, Nat Rev Dis Primers 6(1) (2020) 11.
[27] A.L. Moi, E. Haugsmyr, H. Heisterkamp, Long-Term Study Of Health And Quality Of Life After Burn Injury, Ann Burns Fire Disasters 29(4) (2016) 295-299.
[28] J.W.J. van Kilsdonk, E.H. van den Bogaard, P.A.M. Jansen, C. Bos, M. Bergers, J. Schalkwijk, An in vitro wound healing model for evaluation of dermal substitutes, Wound Repair and Regeneration 21(6) (2013) 890-896.
[29] A.G. Condorelli, M. El Hachem, G. Zambruno, A. Nystrom, E. Candi, D. Castiglia, Notch-ing up knowledge on molecular mechanisms of skin fibrosis: focus on the multifaceted Notch signalling pathway, Journal of Biomedical Science 28(1) (2021) 36.
[30] N.N. Do, S.A. Eming, Skin fibrosis: Models and mechanisms, Current Research in Translational Medicine 64(4) (2016) 185-193.
[31] G.G. Gauglitz, H.C. Korting, T. Pavicic, T. Ruzicka, M.G. Jeschke, Hypertrophic Scarring and Keloids: Pathomechanisms and Current and Emerging Treatment Strategies, Molecular Medicine 17(1) (2011) 113-125.
[32] R.Y. Cheng, G. Eylert, J.-M. Gariepy, S. He, H. Ahmad, Y. Gao, S. Priore, N. Hakimi, M.G. Jeschke, A. Günther, Handheld instrument for wound-conformal delivery of skin precursor sheets improves healing in full-thickness burns, Biofabrication 12(2) (2020) 025002.
[33] D.L. Chester, R.P.G. Papini, Skin and skin substitutes in burn management, Trauma 6(2) (2004) 87-99.
[34] T. Yamamoto, H. Iwase, T.W. King, H. Hara, D.K.C. Cooper, Skin xenotransplantation: Historical review and clinical potential, Burns 44(7) (2018) 1738-1749.
[35] K. Vig, A. Chaudhari, S. Tripathi, S. Dixit, R. Sahu, S. Pillai, V.A. Dennis, S.R. Singh, Advances in Skin Regeneration Using Tissue Engineering, International Journal of Molecular Sciences 18(4) (2017) 789.
[36] Dhasmana, Singh, Kadian, L.K. Singh, Skin Tissue Engineering : Principles and Advances, 2018.
[37] M.P. Rowan, L.C. Cancio, E.A. Elster, D.M. Burmeister, L.F. Rose, S. Natesan, R.K. Chan, R.J. Christy, K.K. Chung, Burn wound healing and treatment: review and advancements, Crit Care 19 (2015) 243.
[38] L. Alrubaiy, K.K. Al-Rubaiy, Skin substitutes: a brief review of types and clinical applications, Oman Med J 24(1) (2009) 4-6.
[39] A.S. Halim, T.L. Khoo, S.J. Mohd Yussof, Biologic and synthetic skin substitutes: An overview, Indian J Plast Surg 43(Suppl) (2010) S23-8.

[40] C.E. Hart, A. Loewen-Rodriguez, J. Lessem, Dermagraft: Use in the Treatment of Chronic Wounds, Adv Wound Care (New Rochelle) 1(3) (2012) 138-141.
[41] E. Foley, A. Robinson, M. Maloney, Skin Substitutes and Dermatology: A Review, Current Dermatology Reports 2(2) (2013) 101-112.
[42] H.R. Ahmadi Ashtiani, M. Akaberi, M.A. Nilforoushzadeh, M. Farahani, Repairing Injured Skin: Biologics, Skin Substitutes, and Scaffolds: Review, 5(4) (2018) e86162.
[43] Y. Wang, J. Beekman, J. Hew, S. Jackson, A.C. Issler-Fisher, R. Parungao, S.S. Lajevardi, Z. Li, P.K.M. Maitz, Burn injury: Challenges and advances in burn wound healing, infection, pain and scarring, Advanced Drug Delivery Reviews 123 (2018) 3-17.
[44] Z. Wang, W. Kapadia, C. Li, F. Lin, R.F. Pereira, P.L. Granja, B. Sarmento, W. Cui, Tissue-specific engineering: 3D bioprinting in regenerative medicine, J Control Release 329 (2021) 237-256.
[45] A.M. Jorgensen, J.J. Yoo, A. Atala, Solid Organ Bioprinting: Strategies to Achieve Organ Function, Chem. Rev. (2020).
[46] L. Moroni, J.A. Burdick, C. Highley, S.J. Lee, Y. Morimoto, S. Takeuchi, J.J. Yoo, Biofabrication strategies for 3D in vitro models and regenerative medicine, Nature Reviews Materials (2018).
[47] C. Mota, D. Puppi, F. Chiellini, E. Chiellini, Additive manufacturing techniques for the production of tissue engineering constructs, Journal of Tissue Engineering and Regenerative Medicine 9(3) (2015) 174-190.
[48] C. Mota, S. Camarero-Espinosa, M.B. Baker, P. Wieringa, L. Moroni, Bioprinting: From Tissue and Organ Development to in Vitro Models, Chem Rev 120(19) (2020) 10547-10607.
[49] R.F. Pereira, P.J. Bartolo, 3D bioprinting of photocrosslinkable hydrogel constructs, J. Appl. Polym. Sci. 132(48) (2015) 42458.
[50] K.S. Lim, J.H. Galarraga, X. Cui, G.C.J. Lindberg, J.A. Burdick, T.B.F. Woodfield, Fundamentals and Applications of Photo-Cross-Linking in Bioprinting, Chem. Rev. (2020).
[51] R.F. Pereira, P.J. Bártolo, 3D bioprinting of photocrosslinkable hydrogel constructs, Journal of Applied Polymer Science 132(48) (2015).
[52] S. Talebian, M. Mehrali, N. Taebnia, C.P. Pennisi, F.B. Kadumudi, J. Foroughi, M. Hasany, M. Nikkhah, M. Akbari, G. Orive, A. Dolatshahi-Pirouz, Self-Healing Hydrogels: The Next Paradigm Shift in Tissue Engineering?, Advanced Science 6(16) (2019) 1801664.
[53] R. Dimatteo, N.J. Darling, T. Segura, In situ forming injectable hydrogels for drug delivery and wound repair, Advanced Drug Delivery Reviews 127 (2018) 167-184.
[54] S. Tavakoli, A.S. Klar, Advanced Hydrogels as Wound Dressings, Biomolecules 10(8) (2020).
[55] P.S. Gungor-Ozkerim, I. Inci, Y.S. Zhang, A. Khademhosseini, M.R. Dokmeci, Bioinks for 3D bioprinting: an overview, Biomaterials Science 6(5) (2018) 915-946.
[56] N.K. Karamanos, A.D. Theocharis, Z. Piperigkou, D. Manou, A. Passi, S.S. Skandalis, D.H. Vynios, V. Orian-Rousseau, S. Ricard-Blum, C.E.H. Schmelzer, L. Duca, M. Durbeej, N.A. Afratis, L. Troeberg, M. Franchi, V. Masola, M. Onisto, A guide to the composition and functions of the extracellular matrix, The FEBS Journal 288(24) (2021) 6850-6912.
[57] J.K. Kular, S. Basu, R.I. Sharma, The extracellular matrix: Structure, composition, age-related differences, tools for analysis and applications for tissue engineering, J Tissue Eng 5 (2014) 2041731414557112.

[58] L.E. Tracy, R.A. Minasian, E.J. Caterson, Extracellular Matrix and Dermal Fibroblast Function in the Healing Wound, Adv Wound Care (New Rochelle) 5(3) (2016) 119-136.
[59] K. Pfisterer, L.E. Shaw, D. Symmank, W. Weninger, The Extracellular Matrix in Skin Inflammation and Infection, Front Cell Dev Biol 9 (2021) 682414.
[60] A. Bandzerewicz, A. Gadomska-Gajadhur, Into the Tissues: Extracellular Matrix and Its Artificial Substitutes: Cell Signalling Mechanisms, Cells 11(5) (2022) 914.
[61] L.G. Griffith, M.A. Swartz, Capturing complex 3D tissue physiology in vitro, Nature Reviews Molecular Cell Biology 7(3) (2006) 211-224.
[62] G.S. Schultz, A. Wysocki, Interactions between extracellular matrix and growth factors in wound healing, Wound Repair and Regeneration 17(2) (2009) 153-162.
[63] J.W. Shin, S.H. Kwon, J.Y. Choi, J.I. Na, C.H. Huh, H.R. Choi, K.C. Park, Molecular Mechanisms of Dermal Aging and Antiaging Approaches, Int J Mol Sci 20(9) (2019).
[64] P. Pittayapruek, J. Meephansan, O. Prapapan, M. Komine, M. Ohtsuki, Role of Matrix Metalloproteinases in Photoaging and Photocarcinogenesis, Int J Mol Sci 17(6) (2016).
[65] H. Laronha, J. Caldeira, Structure and Function of Human Matrix Metalloproteinases, Cells 9(5) (2020).
[66] G. Huang, F. Li, X. Zhao, Y. Ma, Y. Li, M. Lin, G. Jin, T.J. Lu, G.M. Genin, F. Xu, Functional and Biomimetic Materials for Engineering of the Three-Dimensional Cell Microenvironment, Chemical Reviews 117(20) (2017) 12764-12850.
[67] Viscoelastic Biomaterials for Tissue Regeneration, Tissue Engineering Part C: Methods 28(7) (2022) 289-300.
[68] P. Lu, V.M. Weaver, Z. Werb, The extracellular matrix: A dynamic niche in cancer progression, Journal of Cell Biology 196(4) (2012) 395-406.
[69] N. Paxton, W. Smolan, T. Böck, F. Melchels, J. Groll, T. Jungst, Proposal to assess printability of bioinks for extrusion-based bioprinting and evaluation of rheological properties governing bioprintability, Biofabrication 9(4) (2017) 044107.
[70] M.E. Cooke, D.H. Rosenzweig, The rheology of direct and suspended extrusion bioprinting, APL Bioengineering 5(1) (2021) 011502.
[71] X. Zhang, X. Chen, H. Hong, R. Hu, J. Liu, C. Liu, Decellularized extracellular matrix scaffolds: Recent trends and emerging strategies in tissue engineering, Bioactive Materials 10 (2022) 15-31.
[72] Y.S. Kim, M. Majid, A.J. Melchiorri, A.G. Mikos, Applications of decellularized extracellular matrix in bone and cartilage tissue engineering, Bioeng Transl Med 4(1) (2019) 83-95.
[73] M. Gomez-Florit, A. Pardo, R.M.A. Domingues, A.L. Graça, P.S. Babo, R.L. Reis, M.E. Gomes, Natural-Based Hydrogels for Tissue Engineering Applications, Molecules 25(24) (2020).
[74] L.D. Amer, S.J. Bryant, The In Vitro and In Vivo Response to MMP-Sensitive Poly(Ethylene Glycol) Hydrogels, Annals of Biomedical Engineering 44(6) (2016) 1959-1969.
[75] R.F. Pereira, A. Sousa, C.C. Barrias, P.J. Bartolo, P.L. Granja, A single-component hydrogel bioink for bioprinting of bioengineered 3D constructs for dermal tissue engineering, Materials Horizons 5(6) (2018) 1100-1111.
[76] S. Michael, H. Sorg, C.T. Peck, L. Koch, A. Deiwick, B. Chichkov, P.M. Vogt, K. Reimers, Tissue engineered skin substitutes created by laser-assisted bioprinting form skin-like structures in the dorsal skin fold chamber in mice, PLoS One 8(3) (2013) e57741.

[77] P. Admane, A.C. Gupta, P. Jois, S. Roy, C. Chandrasekharan Lakshmanan, G. Kalsi, B. Bandyopadhyay, S. Ghosh, Direct 3D bioprinted full-thickness skin constructs recapitulate regulatory signaling pathways and physiology of human skin, Bioprinting 15 (2019) e00051.
[78] Y. Bin, Z. Dongzhen, C. Xiaoli, E. jirigala, S. Wei, L. Zhao, H. Tian, Z. Ping, L. Jianjun, W. Yuzhen, Z. Yijie, F. Xiaobing, H. Sha, Modeling human hypertrophic scars with 3D preformed cellular aggregates bioprinting, Bioactive Materials 10 (2022) 247-254.
[79] B.S. Kim, M. Ahn, W.-W. Cho, G. Gao, J. Jang, D.-W. Cho, Engineering of diseased human skin equivalent using 3D cell printing for representing pathophysiological hallmarks of type 2 diabetes in vitro, Biomaterials 272 (2021) 120776.
[80] L. Xue, M. Samuel, B. Kapil, F. Marc, S. Min Jae, A biofabricated vascularized skin model of atopic dermatitis for preclinical studies, Biofabrication (2020).
[81] B.S. Kim, G. Gao, J.Y. Kim, D.W. Cho, 3D Cell Printing of Perfusable Vascularized Human Skin Equivalent Composed of Epidermis, Dermis, and Hypodermis for Better Structural Recapitulation of Native Skin, Adv Healthc Mater 8(7) (2019) e1801019.
[82] G. Sriram, M. Alberti, Y. Dancik, B. Wu, R. Wu, Z. Feng, S. Ramasamy, P.L. Bigliardi, M. Bigliardi-Qi, Z. Wang, Full-thickness human skin-on-chip with enhanced epidermal morphogenesis and barrier function, Mater. Today 21(4) (2018) 326-340.
[83] N. Mori, Y. Morimoto, S. Takeuchi, Skin integrated with perfusable vascular channels on a chip, Biomaterials 116 (2017) 48-56.
[84] F. Groeber, M. Holeiter, M. Hampel, S. Hinderer, K. Schenke-Layland, Skin tissue engineering — In vivo and in vitro applications, Advanced Drug Delivery Reviews 63(4) (2011) 352-366.
[85] D. Hao, M. Nourbakhsh, Recent Advances in Experimental Burn Models, Biology (Basel) 10(6) (2021).
[86] T.P. Sullivan, W.H. Eaglstein, S.C. Davis, P. Mertz, THE PIG AS A MODEL FOR HUMAN WOUND HEALING, Wound Repair and Regeneration 9(2) (2001) 66-76.
[87] A.J. Singer, J. Toussaint, W.T. Chung, H.C. Thode, S. McClain, V. Raut, Effects of burn location and investigator on burn depth in a porcine model, Burns 42(1) (2016) 184-189.
[88] M.Å. Andersson, L.B. Madsen, A. Schmidtchen, M. Puthia, Development of an Experimental Ex Vivo Wound Model to Evaluate Antimicrobial Efficacy of Topical Formulations, International Journal of Molecular Sciences 22(9) (2021) 5045.
[89] G.N. Barbalho, B.N. Matos, M.E.L. Espirito Santo, V.R.C. Silva, S.B. Chaves, G.M. Gelfuso, M. Cunha-Filho, T. Gratieri, In vitro skin model for the evaluation of burn healing drug delivery systems, Journal of Drug Delivery Science and Technology 62 (2021) 102330.
[90] N.A. Coolen, M. Vlig, A.J. Van Den Bogaerdt, E. Middelkoop, M.M.W. Ulrich, Development of an in vitro burn wound model, Wound Repair and Regeneration 16(4) (2008) 559-567.
[91] E. Hofmann, J. Fink, A. Eberl, E.-M. Prugger, D. Kolb, H. Luze, S. Schwingenschuh, T. Birngruber, C. Magnes, S.I. Mautner, L.-P. Kamolz, P. Kotzbeck, A novel human ex vivo skin model to study early local responses to burn injuries, Scientific Reports 11(1) (2021) 364.
[92] D. Hao, M. Qu, M. Nourbakhsh, Experimental Study of Burn Damage Progression in a Human Composite Tissue Model, Biology 10(1) (2021) 40.

[93] J.D. Iljas, J. Röhl, J.A. McGovern, K.H. Moromizato, T.J. Parker, L. Cuttle, A human skin equivalent burn model to study the effect of a nanocrystalline silver dressing on wound healing, Burns 47(2) (2021) 417-429.
[94] V. Schneider, D. Kruse, I.B. de Mattos, S. Zöphel, K.K. Tiltmann, A. Reigl, S. Khan, M. Funk, K. Bodenschatz, F. Groeber-Becker, A 3D In Vitro Model for Burn Wounds: Monitoring of Regeneration on the Epidermal Level, Biomedicines 9(9) (2021).
[95] J. Patterson, J.A. Hubbell, Enhanced proteolytic degradation of molecularly engineered PEG hydrogels in response to MMP-1 and MMP-2, Biomaterials 31(30) (2010) 7836-7845.
[96] F. Munarin, M.C. Tanzi, P. Petrini, Advances in biomedical applications of pectin gels, International Journal of Biological Macromolecules 51(4) (2012) 681-689.
[97] M.S.B. Reddy, D. Ponnamma, R. Choudhary, K.K. Sadasivuni, A Comparative Review of Natural and Synthetic Biopolymer Composite Scaffolds, Polymers (Basel) 13(7) (2021).
[98] T. Agarwal, M. Costantini, T.K. Maiti, Extrusion 3D printing with Pectin-based ink formulations: Recent trends in tissue engineering and food manufacturing, Biomedical Engineering Advances 2 (2021) 100018.
[99] S.C. Neves, D.B. Gomes, A. Sousa, S.J. Bidarra, P. Petrini, L. Moroni, C.C. Barrias, P.L. Granja, Biofunctionalized pectin hydrogels as 3D cellular microenvironments, Journal of Materials Chemistry B 3(10) (2015) 2096-2108.
[100] R.F. Pereira, B.N. Lourenço, P.J. Bártolo, P.L. Granja, Bioprinting a Multifunctional Bioink to Engineer Clickable 3D Cellular Niches with Tunable Matrix Microenvironmental Cues, Advanced Healthcare Materials 10(2) (2021) 2001176.
[101] A.J. García, PEG-maleimide hydrogels for protein and cell delivery in regenerative medicine, Ann Biomed Eng 42(2) (2014) 312-22.
[102] D. Kesselman, O. Kossover, I. Mironi-Harpaz, D. Seliktar, Time-dependent cellular morphogenesis and matrix stiffening in proteolytically responsive hydrogels, Acta Biomaterialia 9(8) (2013) 7630-7639.
[103] S. Liu, H. Cao, R. Guo, H. Li, C. Lu, G. Yang, J. Nie, F. Wang, N. Dong, J. Shi, F. Shi, Effects of the proportion of two different cross-linkers on the material and biological properties of enzymatically degradable PEG hydrogels, Polymer Degradation and Stability 172 (2020) 109067.
[104] H. Joodaki, M.B. Panzer, Skin mechanical properties and modeling: A review, Proc Inst Mech Eng H 232(4) (2018) 323-343.
[105] B. Holt, A. Tripathi, J. Morgan, Viscoelastic response of human skin to low magnitude physiologically relevant shear, J Biomech 41(12) (2008) 2689-95.
[106] S. Girardeau-Hubert, B. Lynch, F. Zuttion, R. Label, C. Rayee, S. Brizion, S. Ricois, A. Martinez, E. Park, C. Kim, P.A. Marinho, J.-H. Shim, S. Jin, M. Rielland, J. Soeur, Impact of microstructure on cell behavior and tissue mechanics in collagen and dermal decellularized extra-cellular matrices, Acta Biomaterialia 143 (2022) 100-114.
[107] R.F. Pereira, C.C. Barrias, P.J. Bártolo, P.L. Granja, Cell-instructive pectin hydrogels crosslinked via thiol-norbornene photo-click chemistry for skin tissue engineering, Acta Biomaterialia 66 (2018) 282-293.
[108] Y. Yamaguchi, K. Yoshikawa, Cutaneous Wound Healing: An Update, The Journal of Dermatology 28(10) (2001) 521-534.
[109] J.P.H. Smits, H. Niehues, G. Rikken, I.M.J.J. van Vlijmen-Willems, G.W.H.J.F. van de Zande, P.L.J.M. Zeeuwen, J. Schalkwijk, E.H. van den Bogaard, Immortalized N/TERT keratinocytes as an alternative cell source in 3D human epidermal models, Scientific Reports 7(1) (2017) 11838.

[110] D.E. Ingber, Human organs-on-chips for disease modelling, drug development and personalized medicine, Nature Reviews Genetics 23(8) (2022) 467-491.
[111] D.B. Kolesky, R.L. Truby, A.S. Gladman, T.A. Busbee, K.A. Homan, J.A. Lewis, 3D bioprinting of vascularized, heterogeneous cell-laden tissue constructs, Adv Mater 26(19) (2014) 3124-30.
[112] P. Zoio, A. Oliva, Skin-on-a-Chip Technology: Microengineering Physiologically Relevant In Vitro Skin Models, Pharmaceutics 14(3) (2022).
[113] M. Varkey, D.O. Visscher, P.P.M. van Zuijlen, A. Atala, J.J. Yoo, Skin bioprinting: the future of burn wound reconstruction?, Burns & Trauma 7(1) (2019) 4.